CHALMERS

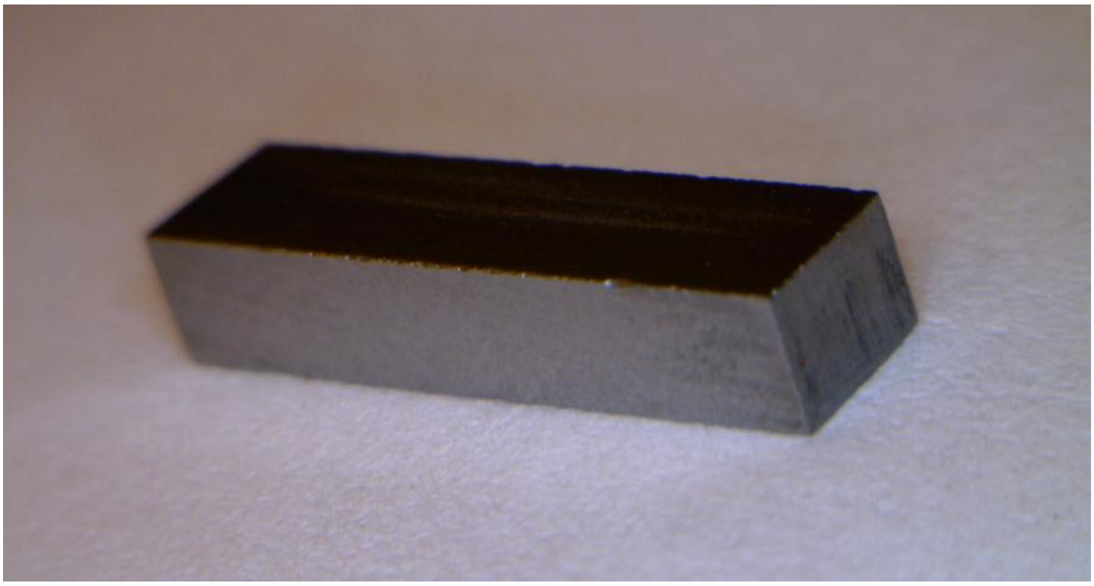

Synthesis and Characterisation of Thermoelectric Clathrate Compounds

Master of Science Thesis [Master Programme Materials and Nanotechnology]

RON CHEUNG

Department of Chemical and Biological Engineering
Division of Applied Surface Chemistry
CHALMERS UNIVERSITY OF TECHNOLOGY
Göteborg, Sweden, 2013

THESIS FOR THE DEGREE OF MASTER OF SCIENCE

Synthesis and Characterisation of Thermoelectric Clathrate Compounds

RON CHEUNG

Supervised by Richard Heijl

Examined by Professor Anders Palmqvist

Department of Chemical and Biological Engineering
Division of Applied Surface Chemistry
CHALMERS UNIVERSITY OF TECHNOLOGY

Göteborg, Sweden, 2013

Synthesis and Characterisation of Thermoelectric Clathrate Compounds

RON CHEUNG

Department of Chemical and Biological Engineering
CHALMERS UNIVERSITY OF TECHNOLOGY
SE-412 96 Göteborg
Sweden
Telephone + 46 (0)31-772 1000

Cover:
[Rectangular bar of $Ba_8Ga_{16}Ge_{30}$ with 2%Sr substituted for Ba, dimensions 2,16x2,88x11,35 mm, cut from spark plasma sintered sample. Picture taken with Dino-Lite Digital Microscope]

Göteborg, Sweden, 2013

Synthesis and Characterisation of Thermoelectric Clathrate Compounds

Ron Cheung
Applied Surface Chemistry
Department of Chemical and Biological Engineering
CHALMERS UNIVERSITY OF TECHNOLOGY

Abstract

Clathrate compounds have recently been studied intensively and shown to possess impressive thermoelectric properties. Studies have shown thermoelectric figure-of-merits among clathrate compounds that are highly competitive with current state-of-the-art thermoelectric semiconductors. Contributing to this is the fact that clathrates have remarkably low thermal conductivity, which is believed to be caused by their caged crystal structure with trapped guest atoms.

In this project, the focus has been on investigating the thermoelectric properties of tin based type VIII clathrate and germanium based type I clathrate, respectively. The clathrates were to be synthesised and characterised and the project was divided into three parts :

1. Tin clathrate $Ba_8Ga_{16-x}Al_xSn_{30}$ with different values on "x" and the effects of the Al substitution of Ga. Due to difficulties with growth of large single crystals using the tin flux method, the task was instead to find a synthesis route for growth of large single crystals followed by finding a method for removal of excess tin.
2. Two phase system $(BaSr)_8Ga_{16}Ge_{30}$ with nanoinclusions of Sr clathrate in the main phase of Ba clathrate and vice versa.
3. Germanium clathrate $Ba_8Ga_{16}Ge_{30}$ with gold nanoinclusion in different concentrations incorporated in the material.

The materials were synthesised using direct heat treatment of high purity elements in vacuum with controlled cooling for crystal growth. The materials were then ball milled to fine powders that were densified into pellets using spark plasma sintering. Analysis methods used were powder X-ray diffraction, transient plane source method for measurements of thermal conductivity and simultaneous measurements of Seebeck coefficient and electrical resistivity.

Crystals of $Ba_8Ga_{16}Sn_{30}$ clathrate were grown from tin flux and excess tin was found possible to remove by diluted nitric acid which, however, also dissolved some of the clathratematerial. Samples of $(BaSr)_8Ga_{16}Ge_{30}$ with different compositions were also synthesised. All samples were sintered to pellets that contained impurity phases like Sn compounds for the $Ba_8Ga_{16}Sn_{30}$ clathrate and Ge and Ga compounds for the $(BaSr)_8Ga_{16}Ge_{30}$ compounds. Results showed some data similar to previously reported but with large variations that possibly indicate low concentration of clathrate structure and disturbance from different impurity phases during measurements.

Keywords: Thermoelectric, Clathrate, Nanomaterial, Nanostructure, Waste heat recovery

Contents

1. Introduction

The thermoelectric effect is a property that some materials have that basically converts a temperature difference into electricity and the other way around using electricity to create a temperature difference. Thermoelectric properties are mainly described by the Seebeck effect, discovered by Seebeck 1821, and the Peltier effect, discovered by Peltier 1834. The Seebeck effect is when a temperature gradient is applied over a thermocouple and then generates a voltage that makes an electric current flow, as an electric generator. The opposite is the Peltier effect when a voltage is applied over a thermocouple so that electric current is running through and heat flow occurs across the thermocouple thus having the effect of a heat pump. The relation between these was later discovered by Thomson, Lord Kelvin 1851, and therefore called the Thomson effect describing the heating or cooling of a conductor having both a current and a temperature gradient. [1] [2]

Thermoelectric devices have been used in different areas for over 40 years, for example in space probes [3] mostly because they are simple, reliable, silent and do not contain moving parts [4]. For long, thermoelectric devices have been made of metals or alloys having low thermoelectric effect and mostly only been used for temperature measuring and sensors but other applications for thermoelectrics have also been developed such as thermoelectric refrigerators [1]. There have been more recent research also in the automobile industry where thermoelectric generators are being evaluated for use to convert waste heat from the engine to electric power and thus to reduce the overall fuel consumption [5], but so far the energy conversion efficiency has not been high enough to motivate the cost of their use in this application. More recent, for about 20 years, research has been made in using new more complex structured materials such as skutterudites, clathrates and other zintl phases [3]. These are materials with complex crystal structures forming large cages that can trap atoms inside whose “rattling” vibrations effectively lower their lattice thermal conductivity giving enhanced thermoelectric properties [6].

The aim of the thesis was to synthesise different clathrate compounds and investigate their thermoelectric properties. The clathrates that were investigated were; $Ba_8Ga_{16}Sn_{30}$ synthesised using the flux method; $(BaSr)_8Ga_{16}Ge_{30}$ two phase system with nanoinclusions of $Sr_8Ga_{16}Ge_{30}$ in $Ba_8Ga_{16}Ge_{30}$ and conversely with $Ba_8Ga_{16}Ge_{30}$ nanoinclusions in $Sr_8Ga_{16}Ge_{30}$ prepared by crystallisation from stoichiometric melt; and also $Ba_8Ga_{16}Ge_{30}$ with different concentrations of gold nanoinclusions, started with stoichiometric crystallisation from melt for making $Ba_8Ga_{16}Ge_{30}$ followed by ball milling to fine powder and precipitation of gold nanoparticles from solution. The compounds were then milled to fine powder and pressed to pellets using spark plasma sintering. The synthesised materials were characterised with X-ray diffraction for structure determination. The properties characterised are the electrical resistivity and the Seebeck coefficient with ULVAC ZEM-3 instrument and thermal conductivity with transient plane source method using Hot Disk instrument.

2. Theory background

The following chapter aims to give some theory for understanding this project and contains relevant background information about thermoelectricity and clathrates.

2.1. Thermoelectric effect

A thermoelectric device is made of many thermocouples linked together thermally in parallel and electrically in series. Each thermocouple is made of two elements of different type, n-type having free negative electrons and p-type having free positive holes as charge carriers, as shown schematically in Figure 1. [3] When a temperature difference is applied over the two junctions of the thermocouple, the charge carriers tend to move from the hot side to the cold side of the material, described by the Seebeck effect, and a voltage is created that drives an electric current through the thermocouple in the electrical circuit, Figure 1 (a). The contrary occurs when an external voltage is applied to the circuit driving a current, and a heat difference is created, Figure 1 (b). [1]

The Seebeck coefficient α, sometimes also called thermopower or denoted S, is given by

$$\alpha = \frac{\Delta V}{\Delta T}$$

measured in $\mu V/K$ and where ΔT is the temperature difference over the material and ΔV the induced voltage. The coefficient is negative for n-type materials and positive for p-type materials. [1]

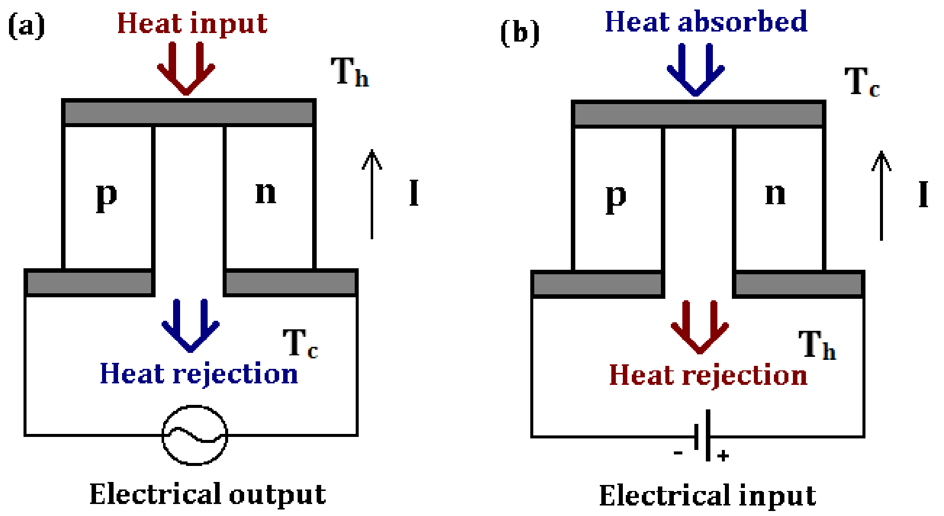

Figure 1. Schematic figure of thermocouples with a p-type and a n-type element, a hot and a cold side with temperature T_h and T_c respectively, and a) for Seebeck effect where a current is driven by the temperature gradient and b) for Peltier effect where heat is pumped across the thermocouple driven by an external electrical power input. (After reference [1])

The opposite effect is described by the Peltier effect when an external electric power is applied on the thermocouple and heat is pumped from one side to another, giving the Peltier coefficient :

$$\pi = \frac{q}{I}$$

where I is the applied current and q is the heat rate transported over the thermocouple (heating rate q at one side and cooling rate $-q$ at the opposite side). [1]

The conversion efficiency of thermoelectric materials is defined by a dimensionless thermoelectric figure of merit described as :

$$zT = \frac{\alpha^2}{\rho\kappa}T \left(= \frac{\alpha^2\sigma}{\kappa}T\right)$$

where α is the Seebeck coefficient, T is the temperature, ρ is the electrical resistivity, and κ is the thermal conductivity, (σ is the electrical conductivity). A larger figure of merit gives better thermoelectric efficiency, thus much research aims to maximise this while so far the figure of merit has typically been measured to around 1 for the best materials. [3]

The thermal conductivity has two contributing parts, the heat transport through electrons (κ_e) and the heat transport via phonons in the lattice (i.e. crystal vibrations) (κ_l) :

$$\kappa = \kappa_e + \kappa_l$$

The thermal conductivity from electrons (κ_e) can be related to the electrical conductivity (σ) from the Wiedemann-Franz law :

$$\kappa_e = L\sigma T$$

where L is the Lorenz number. Increasing the electrical conductivity thus results in increased electrical thermal conductivity. [3] [7]

For a thermoelectric material under a temperature gradient, the charge carriers, both electrons and holes, are moving from the hot side towards the cold side as mentioned before. Thus, in order to have a strong Seebeck effect, each material could only contain one type of carrier.

The electrical conductivity (σ) is related to the charge carrier concentration (n) and the carrier mobility (μ) as shown in the following equation:

$$\sigma = ne\mu$$

The properties' dependence on the charge carrier concentration is shown schematically in Figure 2. With increasing charge carrier concentration it follows that; the electronic part of thermal conductivity (κ_e) is increasing giving increased thermal conductivity (κ), the electrical conductivity (σ) is increasing while the Seebeck coefficient (α) is decreasing. Since increased thermal conductivity lowers the figure of merit while the electrical conductivity increases it, a balance between the properties has to be found while optimising the figure of merit. [1] [3]

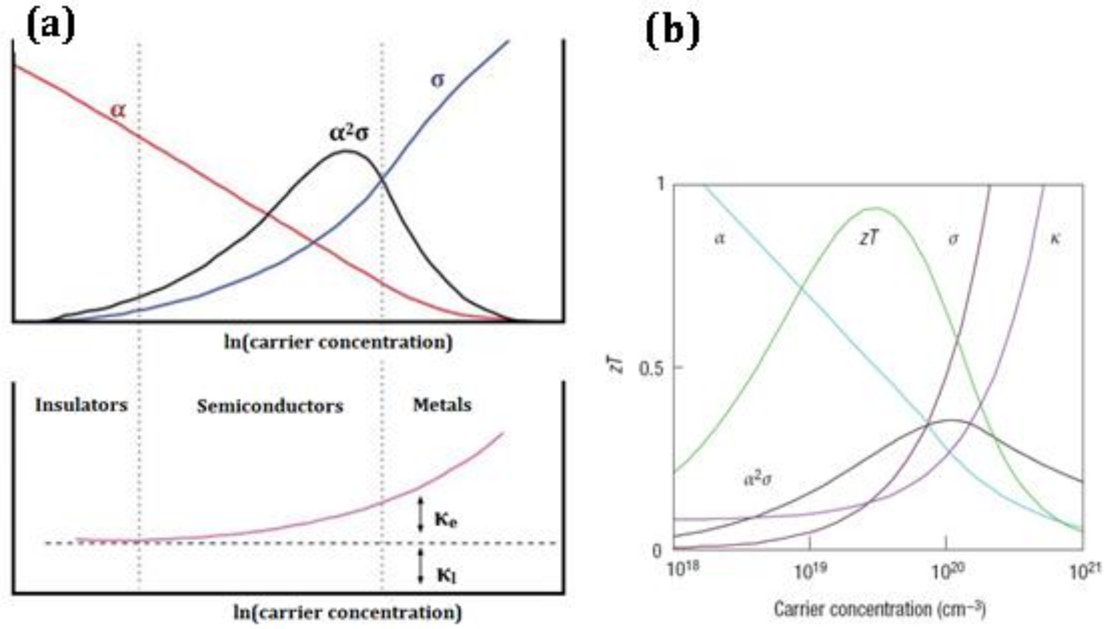

Figure 2. The dependence of charge carrier concentration for the Seebeck coefficient (α), thermoelectric power factor ($\alpha^2\sigma$), electrical conductivity (σ), and (a) also the electrical thermal conductivity (κ_e) and lattice thermal conductivity (κ_l) [1] [8], (b) also total thermal conductivity (κ) and dimensionless figure of merit (zT) [3]

2.2. Clathrates

Clathrates are solid materials with a host-quest crystal structure. The crystal structure consists of host atoms that form cages that host guest atoms. The two different atom types interact with each other via weak forces and the guest atoms should be significantly smaller than the cage but large enough to be trapped [9] [10]. The size ratio between the guest atoms and the cages allows the trapped atoms to move inside the cages creating a rattling effect which has been proposed to scatter phonons of different wavelengths leading to lowered lattice thermal conductivity [6]. More recent explanations for the low thermal conductivity of clathrates refer to a decreased phonon group velocity.

There are several different types of clathrates and for thermoelectric applications mostly clathrates of type I with cubic crystal structure $\mathrm{Pm\bar{3}n}$ with the chemical formula $\mathrm{A_8^{II}B_{16}^{III}B_{30}^{IV}}$ has been studied. In the formula A^{II} = Ba, Sr (group two elements) are the trapped guest atoms, B^{III} = Al, Ga (group three elements) and B^{IV} = Si, Ge, Sn (group four elements) are the atoms constituting the cage structure. An example is the compound $Ba_8Ga_{16}Ge_{30}$ that has type I clathrate structure where the host atoms are tetrahedrally bonded forming polyhedra cages with 20 (dodecahedron) and 24 (tetrakaidecahedron) coordinated atoms. [6] [9] A different kind of clathrate is the type VIII structure that could be formed by for example $Ba_8Ga_{16}Sn_{30}$, and has the same chemical formula as type I clathrates but the space group is $I\bar{4}3m$ and the guest atoms are filling only one type of cages that are made of 23 coordinated atoms (a distorted dodecahedron with additional bonds). Figure 3 illustrates the different cage structures of the clathrate type I (a) and type VIII (b), respectively. [11]

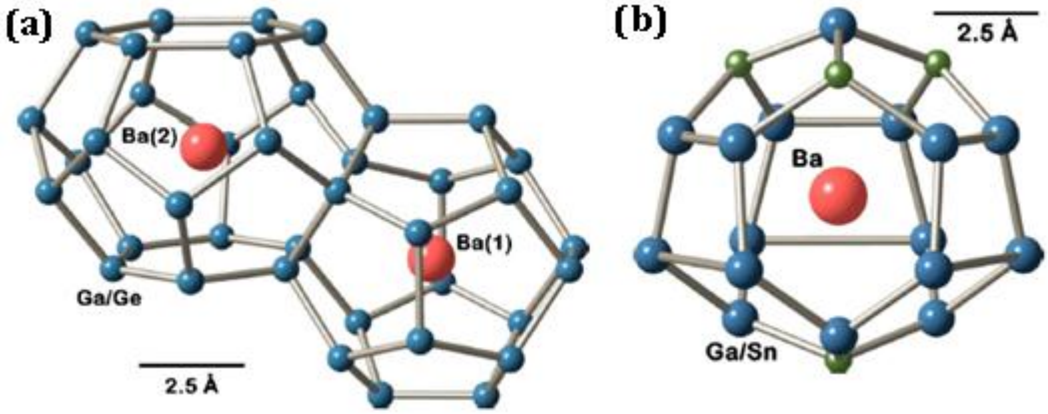

Figure 3. (a) The cage structures of clathrate type I formed by $Ba_8Ga_{16}Ge_{30}$ with the tetrakaidecahedron cage formed by 24 Ga and Ge atoms to the left and the dodecahedron cage formed by 20 atoms to the right. (b) The cage structure of clathrate type VIII formed by $Ba_8Ga_{16}Sn_{30}$ an irregular cage formed by 23 atoms. All cages with Ba trapped inside. [12]

2.3. Nanostructured materials

Structuring thermoelectric materials in the micro- and nanometer scale may potentially increase their thermoelectric effect. The smaller scale for the material's particles means increased concentrations of interfaces that scatter phonons and lowers the thermal conductivity with potential to increase the figure of merit. Also having the particles of different size ranges increases the scattering over different wavelengths, which contributes to further lowered thermal conductivity. It is desirable when possible to improve for example the thermal properties without distorting the electrical properties. There are several different ways of synthesising nanostructured thermoelectric materials, for example precipitating different compounds in solution or precipitations of compounds from solidification of molten material. The material could also be milled to fine powders, mixed with nanoparticles or nanocrystals and densified by applying high pressure to the material. [8] [13] [14] [15]

3. Experimental methods

This part is structured to first give a theoretical summary for the different techniques that are used, followed by the details for the experimental part conducted, including synthesis, sample preparation and characterisation.

3.1. Synthesis

3.1.1. $Ba_8Ga_{16}Sn_{30}$

One of various methods for synthesis of materials is the flux method which is a form of solution synthesis. In solution synthesis the precursors are dissolved in a solvent and when a metal is used as solvent it is called a flux. The mixture is then heated in a furnace to an elevated temperature required for the reaction to take place and then cooled slowly so that crystals will form and then be separated from the solvent or flux by pouring it off or using other available methods. This method is likely to form large single crystals with defined facets. [16]

Samples of $Ba_8Ga_{16}Sn_{30}$ were prepared in an argon filled glove box where high purity elements of Ba, Ga and Sn were weighed and mixed in an alumina crucible (~30 mm diameter, ~60 mm height) and sealed in a quartz tube (~4 cm inner diameter, ~44 cm total length), evacuated and put in a vertical tube furnace, a Thermolyne 21100 with Eurotherm controller. The sample was heated to elevated temperature and cooled with controlled cooling rates for growth of single crystals.

The first batch of $Ba_8Ga_{16}Sn_{30}$ was prepared with starting materials Ba:Ga:Sn in ratios 8:30:50, from 10.967 g Sn (99.999%, 3mm shots, Alfa Aesar), 2.05319 g Ga (99.9995%, liquid, Sigma Aldrich) and 2.010 g Ba (99.99%, dendritic pieces, Sigma Aldrich). The material was heated to 490 °C over 10 h and kept there for 10 h, cooled to 390 °C over 50 h and cooled to 25 °C over 8 h, as in reference [17] where the melting point for the compound was found to be 514 °C. Slow cooling to room temperature was added to prevent any cracking of samples or crucible if cooled too fast. The same batch was taken out and then resealed in the quartz tube and heat treated again with the same program but increased cooling time to 80 h between 490 °C and 390 °C, the increased cooling time was intended for growth of large single crystals which was not successful in the first heat treatment cycle. Details for the synthesis are presented in Appendix A – Synthesis.

3.1.2. $(BaSr)_8Ga_{16}Ge_{30}$ two phase system

A compound was to be synthesised as a two phase system of two different clathrates, having one as the main phase with nano precipitates of the other clathrate. One compound was chosen to be $Ba_8Ga_{16}Ge_{30}$ and the second clathrate should preferably be a similar type I clathrate compound that has elements substituted but having a cell parameter as close to that one for $Ba_8Ga_{16}Ge_{30}$ as possible hoping to be able to synthesise the material with a more uniform crystal structure.

Cell parameters for $Ba_8Ga_{16}Ge_{30}$ and some other clathrates were found in the published literature. The data are experimental values and mostly from X-ray diffraction at room temperature or near room temperature for the comparability and are presented below in Table 1. The clathrate $Sr_8Ga_{16}Ge_{30}$ had the cell parameter most similar to $Ba_8Ga_{16}Ge_{30}$ thus more references were investigated for higher reliability, and this compound was chosen to be synthesised together with $Ba_8Ga_{16}Ge_{30}$. A brief research [9] [10] [18] [19] [20] [21] of the compounds thermoelectric properties showed that $Ba_8Ga_{16}Ge_{30}$ and $Sr_8Ga_{16}Ge_{30}$ have similar values of α and κ but $Ba_8Ga_{16}Ge_{30}$ has slightly higher zT-value. The melting temperature is 974 °C for $Ba_8Ga_{16}Ge_{30}$ and 774 °C for $Sr_8Ga_{16}Ge_{30}$ [9] and are used for determining the heating scheme for the synthesis which will include one cooling ramp at each melting temperature, faster cooling for the precipitated phase and slower cooling for the main phase.

Table 1. Literature data of cell parameter for different type I clathrate compounds.

Clathrate	$\mathbf{Ba_8Ga_{16}Ge_{30}}$	$\mathbf{Sr_8Ga_{16}Ge_{30}}$	$\mathbf{Ba_8Al_{16}Ge_{30}}$	$\mathbf{Ba_8In_{16}Ge_{30}}$	$\mathbf{Ba_8Ga_{16}Si_{30}}$	$\mathbf{Ba_8Al_{16}Si_{30}}$	$\mathbf{Sr_8Ga_{16}Si_{30}}$	$\mathbf{Sr_8Al_{16}Si_{30}}$
a, (Å)	10.76035[22] 10.785[23] 10.7802[24] 10.7815[24] 10.7822[24] 10.7828[25] 10.785[26] 10.786[27] 10.7668[28] 10.739[9] 10.7844[29]	10.7274[22] 10.74[23] 10.73[6] 10.73637[30] 10.7343[28] 10.719[9]	10.8518[31] 10.84865[32] 10.835[28]	11.1175[22] 11.2177[31]	10.4432[22] 10.509[9] 10.53[28]	10.6068[28]	10.4595[28]	10.4767[28]

A simple way of reacting materials is solid state synthesis that could be done by heat treating stoichiometric amounts of starting material in a controlled atmosphere or vacuum. The temperature is increased to below the melting point of the compounds and held until the elements react and then cooled at controlled rate for possibly crystal growth. Alternatively the temperature is raised further in the beginning for melting the starting material and achieve proper mixing before the cooling step. [16]

Compounds of $(BaSr)_8Ga_{16}Ge_{30}$ were synthesised both with having Ba clathrate in the main phase and the reversed case having Sr clathrate in the main phase. The Sr substitutions of Ba were in concentrations 2mol% and 4mol% and vice versa, and reference samples of $Ba_8Ga_{16}Ge_{30}$ and $Sr_8Ga_{16}Ge_{30}$ were also synthesised. High purity elements of Ba, Sr, Ga and Ge were mixed in stochiometric ratios in an alumina crucible sealed under argon atmosphere, evacuated and heated in tube furnace. The synthesis route for $Ba_8Ga_{16}Ge_{30}$ 2%Sr was as follows: the material was heated to 1050 °C, dwelled for an hour, cooled to first 980 °C then to 963 °C and dwelled for 36 h, then cooled to 930 °C and to 780 °C, then slowly cooled to 730 °C and then to room temperature. These heating and cooling rates were determined by modifying the synthesis route for Ba clathrate [33] by adapting to the melting point for Sr clathrates and with estimated cooling rates which also varied some depending on the concentrations of the different compounds and batches. Details for all synthesised compounds are presented in Appendix A – Synthesis.

3.1.3. $Ba_8Ga_{16}Ge_{30}$ with gold nanoinclusions

$Ba_8Ga_{16}Ge_{30}$ was prepared with high purity elements of Ba, Ga, Ge weighed in stoichiometric ratio with additional 2.5 mol% excess Ba to compensate the typical Ba loss during the sintering. The starting material was prepared in the same way as mention before with similar heating and cooling treatment as for the $(BaSr)_8Ga_{16}Ge_{30}$ samples.

Four batches of $Ba_8Ga_{16}Ge_{30}$ were prepared and they were ball milled to powder that was sieved to obtain uniform particle size ≤ 32 µm, and then the batches were mixed together into one common batch.

The fine $Ba_8Ga_{16}Ge_{30}$ powder was divided into four samples à 7.0 g. Gold nanoparticles were introduced to these powders by precipitation resulting in a series of samples with different concentrations of gold inclusions, one reference without addition of gold particles and three with gold concentrations of 0.4, 0.8 and 1.2 vol%, respectively. For this, gold(III)chloride trihydrate was dissolved in ~ 14 ml ethanol (99.5 %). The solution was dropped in small amounts onto the $Ba_8Ga_{16}Ge_{30}$ powder placed on a glass dish on a heating plate (50 - 80 °C) under continuous stirring with a glass rod. When the ethanol had evaporated the powder was let to dry on the glass plate for approximately three hours.

3.2. Sample Preparation

Spark plasma sintering is a method where the powder is put into a die and high pressure is applied at the same time as a pulsed direct current is sent through the die and sample heating it up rapidly. The powder is compacted to a density as high as 95 - 100% of theoretical value. [14] [15]

All samples were ball milled with Retsch Mixer Mill MM 400 with a grinding jar of ZrO_2 (25 ml), grinding ball (15 mm diameter) and using grinding times 10 - 60 min with frequencies 14 – 17 Hz several times and in different portions. The powders with particle size ≤ 32 µm were spark plasma sintered, at Aarhus University Denmark, into cylindrical pellets of approximately 13 mm diameter and 5 - 6 mm thick. When possible, the samples were cut into two discs, with a Model 660 Low Speed Diamond Wheel Saw from South Bay Technology Inc., for thermal property measurements. The same samples were subsequently cut into rectangular bar shapes for Seebeck coefficient and electrical resistivity measurements.

3.3. Characterisation

The methods used and details for characterisation of the materials are presented in this part.

3.3.1. Powder X-ray Diffraction

Crystals are formed by identical atoms or groups of atoms as building blocks that are arranged in a periodic array in three dimensions, except for any defects or impurities that may occur [7]. If a compound of crystal structure is finely ground to powder it will be composed of many small crystals that are all randomly oriented. In powder X-ray diffraction, PXRD, a monochromatic X-ray beam is run through the powder sample letting the crystals oriented in different directions diffract the beam. The X-ray source, the sample and detector are rotated to form different angles to detect the intensities of diffraction [16]. The X-ray beam is diffracted when reflected on the crystal planes and constructive interference occurs for specific angles that form between the radiation beam and the crystal planes, Figure 4. This follows the Bragg law:

$$2d\,sin\,\theta = n\lambda$$

where d is the spacing between the crystal planes, θ the angle between the radiation beams and the crystal plane, n is the order of diffraction and λ the wavelength and which also has to fulfil the criteria $\lambda \leq 2d$. [7]

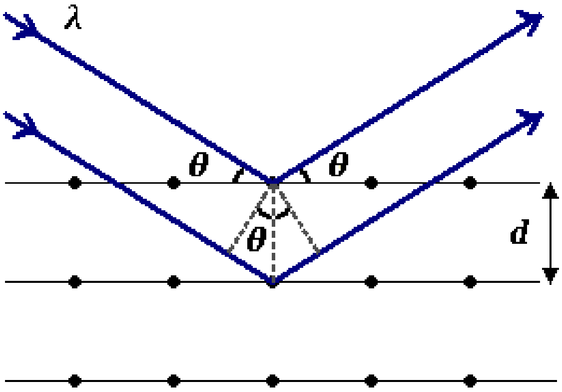

Figure 4. Diffraction of the X-ray beams with wavelength *λ* against crystal planes with spacing *d* forming the angle *θ*. (After reference[16])

The products were characterised using powder X-ray diffraction with a Bruker D8 Advance diffractometer with a Cu-Kα source λ = 1.5418 Å and a LynxEye detector. Measurement performed on angles 2θ between 20° and 60° with uniform steps for 15 minutes at room temperature. The diffraction data were analysed with the EVA software. After the powders were sintered to pellets they were characterised again, analysed with the same settings but on a polished surface of the pellet.

3.3.2. Transient Plane Source method

Transient Plane Source (TPS) method is a technique that from a single measurement can give a materials thermal conductivity, thermal diffusivity and specific heat per unit volume. The

TPS method is based on a sensor that is being heated by short pulses of electric current sent through it. The sensor is usually made of a thin double spiral of electrically conducting material that is surrounded by thin sheets of supporting and electrically insulating material. The sensor is put between two pieces of sample with flat surfaces and the sample will get heated by the sensor that both acts as a heat source and a thermometer, measuring the resistance multiple times for a specific amount of time. With known temperature coefficient (TCR) for the sensor materials, the resistance measurements give a temperature change as function of time. [34]

The thermal properties of the materials were analysed with a Hot Disk Thermal Constant Analyser TPS 2500 S using the Hot Disk Thermal Constant Analyser Software Version 7.0.10. The Hot Disk sensor used, model C5465 3.189 mm radius, was with a nickel double spiral covered with two sheets of Mica material for measurements in a tube furnace from Entech Ängelholm Sweden with a Eurotherm 2416 controller. Measurements were performed between 50 - 450 °C with a measuring time of 2 seconds, applied power varying between 150 - 350 W for different samples and 5 measurements with 15 minutes between each, at each temperature. $Ba_8Ga_{16}Ge_{30}$ was measured with the sensor between two pieces of samples while the other materials were measured single sided, meaning the sensor was placed between a sample on one side and insulating material, glass fibre, on the other side. Thermal properties of the glass fibre were measured at room temperature with a kapton sensor, used in the calculations.

3.3.3. Seebeck coefficient and electrical resistivity measurements

The Seebeck coefficient is measured by placing the sample material at a certain temperature and also under a temperature gradient and by measuring the voltage along the same direction, the ratio between the voltage and the temperature difference gives the Seeebeck coefficient. For electrical resistivity measurements a current (I) is driven through the sample and the voltage (ΔV) is measured between two points over a sample with known dimensions and the resistivity (ρ) could be calculated with the following equation

$$\rho = \frac{\Delta V}{I} \times \frac{A}{L}$$

where *A* is the cross section area of the sample and *L* the distance between the points of measurement. [35] [36]

The Seebeck coefficient and electrical resistivity were measured simultaneously with a ZEM-3 ULVAC-RICO. For Seebeck coefficient measurements the samples are put under a temperature gradient while the probes are in contact with the sample at two points measuring the temperatures and voltage difference. For resistivity measurements a four point probe method is used where the probes measures the voltage different over the sample while a current is sent through. For a schematic illustration of the experimental setup for the ZEM-3, see Figure 5. [37] [38]

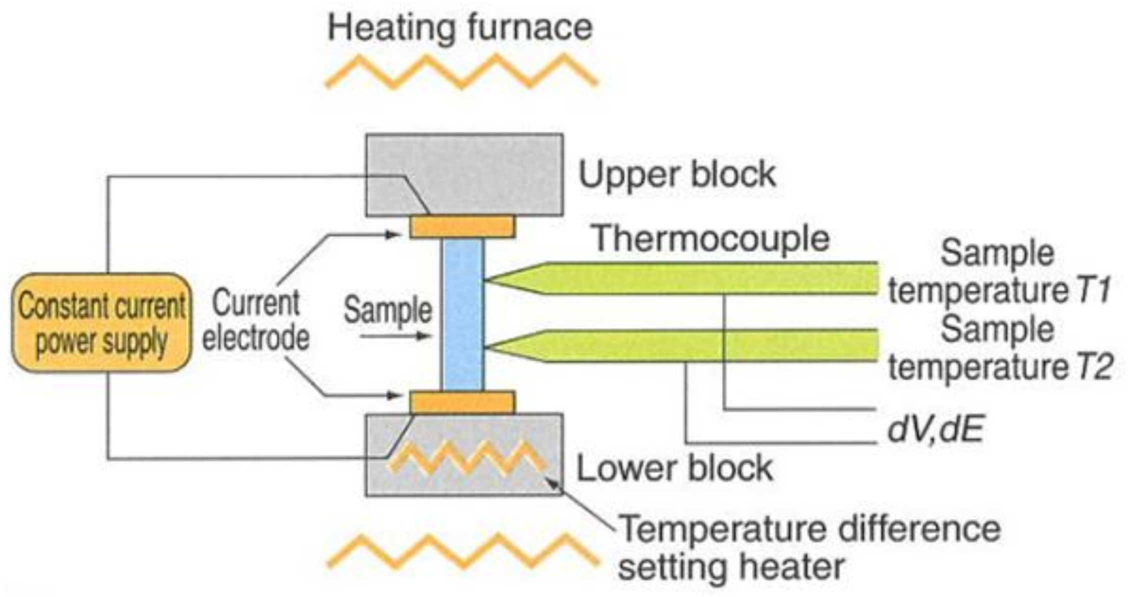

Figure 5. Schematic representation of the measuring device in the ZEM-3 for simultaneous measurements of Seebeck coefficient and electrical resistivity. [38]

Seebeck coefficient and electrical resistivity measurements were performed on samples cut into rectangular bar shapes. The measurements were done between 30 °C – 450 °C where experimental data were collected for temperature gradients of 20 °C, 30 °C and 40 °C at certain temperature measuring points in a low pressure helium atmosphere. For detecting any hysteresis the measurements were performed both during heating and cooling of sample.

4. Results

The results are presented in this chapter and the measurement data could be found in Appendix B – Results.

4.1. $Ba_8Ga_{16}Sn_{30}$

Since the flux method was used for synthesis, there was excess tin along with the samples that needed to be removed. One large single crystal (irregular shape of ~4 mm thick and ~21 mm wide at its largest) was obtained from which the excess tin was surrounding the crystal, making it possible to simply in a careful and controlled way push and scrape the tin away with a spatula. Most of the tin came off revealing the single crystal with clear visible faceted edges, Figure 6. For other samples where the crystals were smaller, some tin could be melted and scraped away but this was not very successful since molten tin does not just run off. Concentrated hydrochloric acid (HCl 37%) at room temperature dissolved the tin and possibly also the clathrates, but the reaction was too slow thus not an option. However, diluted nitric acid (HNO_3 ~35%) dissolved the tin in circa 1 hour, along with some of the clathrate. After washing the crystals with water and alcohol the crystals looked shiny and without tin on the surface. Powder from two different batches were mixed together and resulted in one piece of sintered pellet.

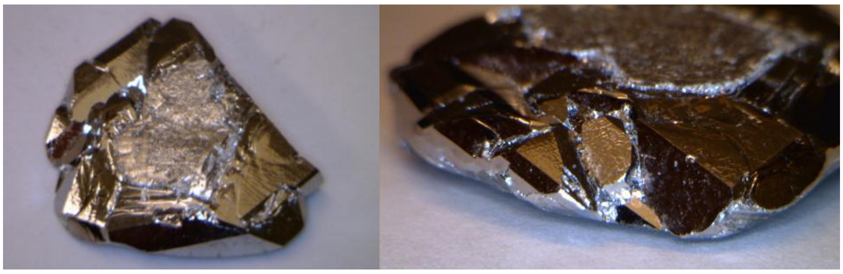

Figure 6. Grown $Ba_8Ga_{16}Sn_{30}$ single crystal with some tin remaining on some parts of the surface. Dimension approximately 21 mm wide and 4 mm thick.

During measurements of Seebeck coefficient and electrical resistivity, the single crystal sample piece had an edge from which tin melted and leaked from. This has probably affected the measurements and the results. The sintered $Ba_8Ga_{16}Sn_{30}$ sample was <6 mm thick thus was not possible to cut into two discs. During TPS measurements the pellet leaked some tin compounds, however when cut into rectangular bar it revealed no cracks inside the pellet but more tin was leaking from the sample surfaces during Seebeck coefficient and electrical resistivity measurements.

Figure 7 shows the X-ray diffractograms of the $Ba_8Ga_{16}Sn_{30}$ samples prepared which corresponds to results shown in reference [17]. The data were collected from different batches prepared and in different stages of the sample preparation. One is from a piece from the single crystal mentioned above with as much tin removed from the surfaces as possible by polishing with sandpaper. Results show clear clathrate structure but with traces of tin compound. Another sample batch with diffractograms both before and after that excess tin was removed from the crystal by treatment with acid, showing that the tin content has not significantly been reduced. Finally the diffractogram of a spark plasma sintered pellet shows decreased clathrate structure but increased tin content along with some graphitic carbon and small traces of barium, compared to before sintering. The carbon comes from the die used for sintering and is left surrounding the pellet on its surfaces.

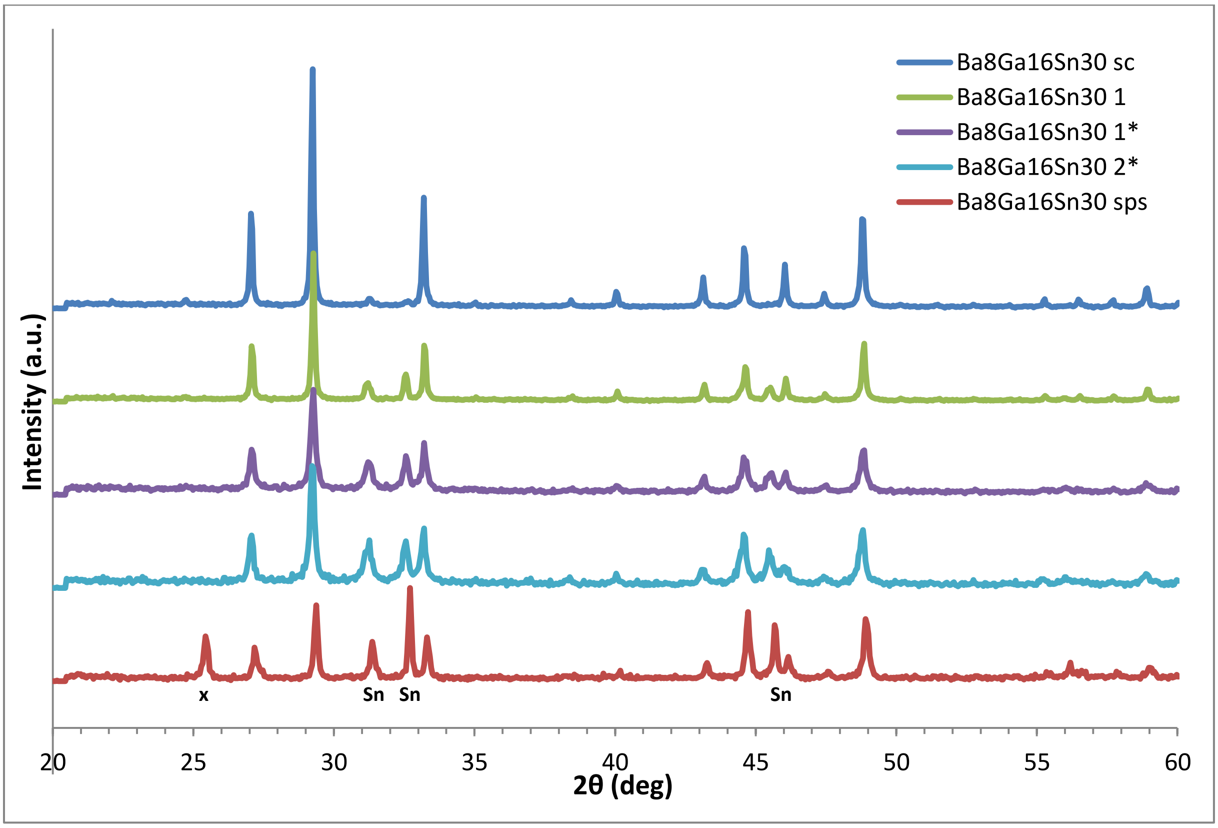

Figure 7. X-ray diffractograms of prepared $Ba_8Ga_{16}Sn_{30}$ samples. Powder diffraction data; "sc" denotes a single crystal sample, samples 1 and 2 are sample batches with small crystals, samples marked with "*" are samples having tin removed with acid treatment. Sample "sps" denotes data collected from sintered pellet of a polished surface. The peak marked with "x" mostly represents carbon (graphite) but also some Ba. Peaks for the tin are marked with Sn.

Results from measured properties for $Ba_8Ga_{16}Sn_{30}$ samples are presented in Figure 8. The electrical resistivity, Figure 8 (a), was ca 5.5 – 8.3 mΩcm for the single crystal sample and lower for the sintered sample, ca 2.5 – 5.4 mΩcm, between 30 and 350 °C. The resistivity for the single crystal sample matches those previously reported to ca 4.5 – 6.5 mΩcm between 27 – 227 °C [39] and ca 5 – 8 mΩcm between 27 – 327 °C [17] [40] [41]. The Seebeck coefficient, Figure 8 (b), was measured to be at largest around -240 µV/K at ca 250 °C, which is similar to results reported by reference [39] between -190 and -250 µV/K at temperatures 27 – 277 °C but lower than results from references [17] [40] [41] between -240 and -320 µV/K at 27 – 327 °C. The measured value for the sintered sample was below -30 µV/K. The measured thermal conductivity of the sintered $Ba_8Ga_{16}Sn_{30}$, Figure 8 (d), stays around 2.5 W/mK at temperatures 30 – 350 °C. These results do not correspond to the value reported previously in references where the laser flash method was used given values of ca 0.7 - 1.4 W/mK between 27 - 327 °C [17] [40] [41], of which values from reference [17] is included as “Ba8Ga16Sn30 ref” in Figure 8 (d) with extrapolated value at 350 °C.

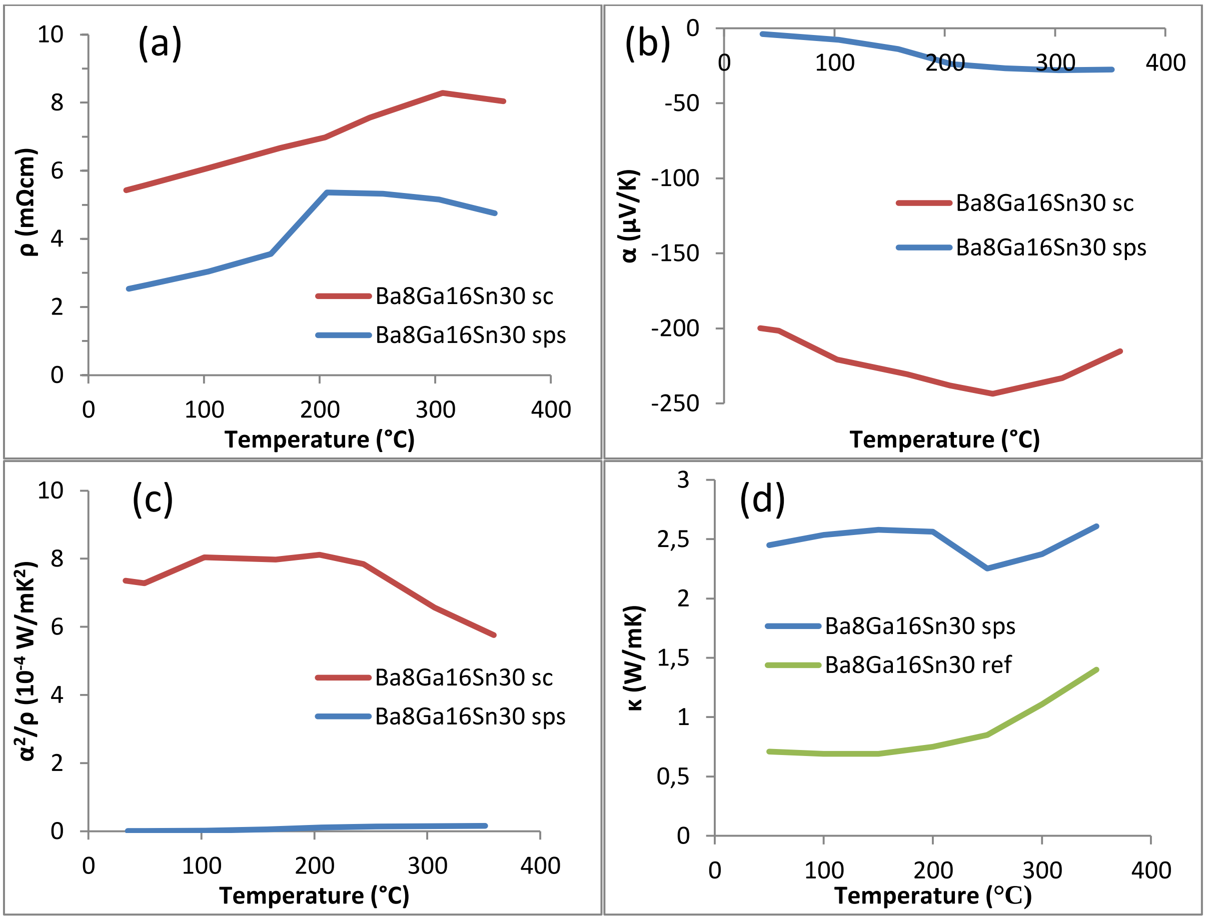

Figure 8. Measured properties as function of temperature for synthesised $Ba_8Ga_{16}Sn_{30}$ single crystal, sample marked “sc”, and spark plasma sintered sample marked “sps”. (a) Electrical resistivity. (b) Seebeck coefficient. (c) Power factor, α^2/ρ. (d) Thermal conductivity, “ref” was values taken from reference [17].

The dimensionless figure of merit for the sintered $Ba_8Ga_{16}Sn_{30}$ sample is shown in Figure 9 where a maximum of 0.087 is reached at 250 °C. This value is slightly lower than those reported to ca 0.8 at temperatures around 200 °C [17] [40] [41], which show that at least the temperature interval at which maximum value is reached and the trend of the curve is the same. The figure of merit for the single crystal sample was calculated with thermal conductivity from reference [17] and shows a maximum value of 0.23 at 250 °C, also lower than reference values but higher than for the sintered sample.

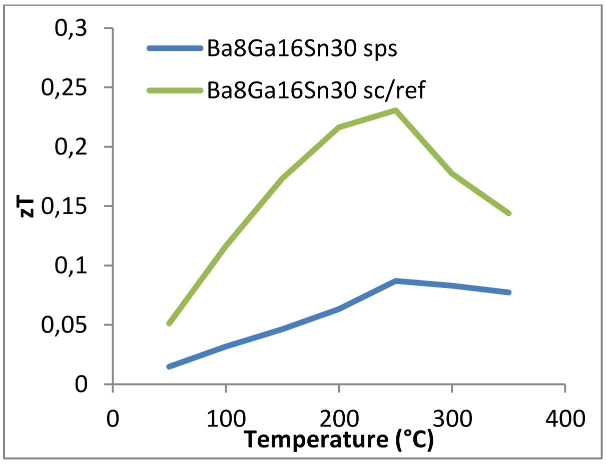

Figure 9. Dimensionless figure of merit for sintered $Ba_8Ga_{16}Sn_{30}$ sample. For single crystal sample values were calculated with measured power factor but thermal conductivity taken from reference [17].

4.2. $(BaSr)_8Ga_{16}Ge_{30}$

The sintered sample of $Ba_8Ga_{16}Ge_{30}$ showed multiple cracks in the pellet which also finally broke after measurements. $Ba_8Ga_{16}Ge_{30}$ 2%Sr had a few cracks in the pellet but the sample was enough for measurements, unlike $Ba_8Ga_{16}Ge_{30}$ 4%Sr which was only sufficient for Seebeck coefficient and electrical resistivity measurements. The samples of $Sr_8Ga_{16}Ge_{30}$, $Sr_8Ga_{16}Ge_{30}$ 2%Ba and $Sr_8Ga_{16}Ge_{30}$ 4%Ba all showed leakage of Ga, and were thus heat treated at 450 °C for 24 h after which some Ga content was removed to avoid this problem during measurements. Despite this more Ga was leaking during measurements. These pellets were fine with either only minor cracks or no cracks at all.

X-ray diffractograms of synthesised compounds are shown in Figure 10, where (a) – (c) are for compound $Ba_8Ga_{16}Ge_{30}$, $Ba_8Ga_{16}Ge_{30}$ 2%sr and 4%Sr substituted, respectively and (d) – (f) are for compound $Sr_8Ga_{16}Ge_{30}$, $Sr_8Ga_{16}Ge_{30}$ 2%Ba and 4%Ba substituted, respectively. The diffractograms show both powder diffraction data for the synthesised materials and the diffraction data collected from surfaces of spark plasma sintered pellets. For the Sr clathrate compounds, (d) – (f), include diffractograms from the sintered pellets after they were heat treated for removal of gallium compound. The diffractograms show clathrate structures that correspond to that of $Ba_8Ga_{16}Ge_{30}$ and $Sr_8Ga_{16}Ge_{30}$, respectively. These are both rather similar to each other along with the low concentration of the substituted amounts during synthesis, no apparent signs of these substitutions are visible in these X-ray diffractograms. All the synthesised powders, before spark plasma sintering, show clear clathrate structure with amounts of Ge compound included. After sintering, the $Ba_8Ga_{16}Ge_{30}$ based compounds, Figure 10 (a) – (c), show decreased concentration of clathrate structure and an increased amount of a Ge phase. For the $Sr_8Ga_{16}Ge_{30}$ based compounds, (d) – (f), the contents of Ge in the sintered samples have greatly increased compared to the clathrate structure that has been significantly reduced. For all sintered samples there is a peak that shows carbon presence which is from the die used for spark plasma sintering.

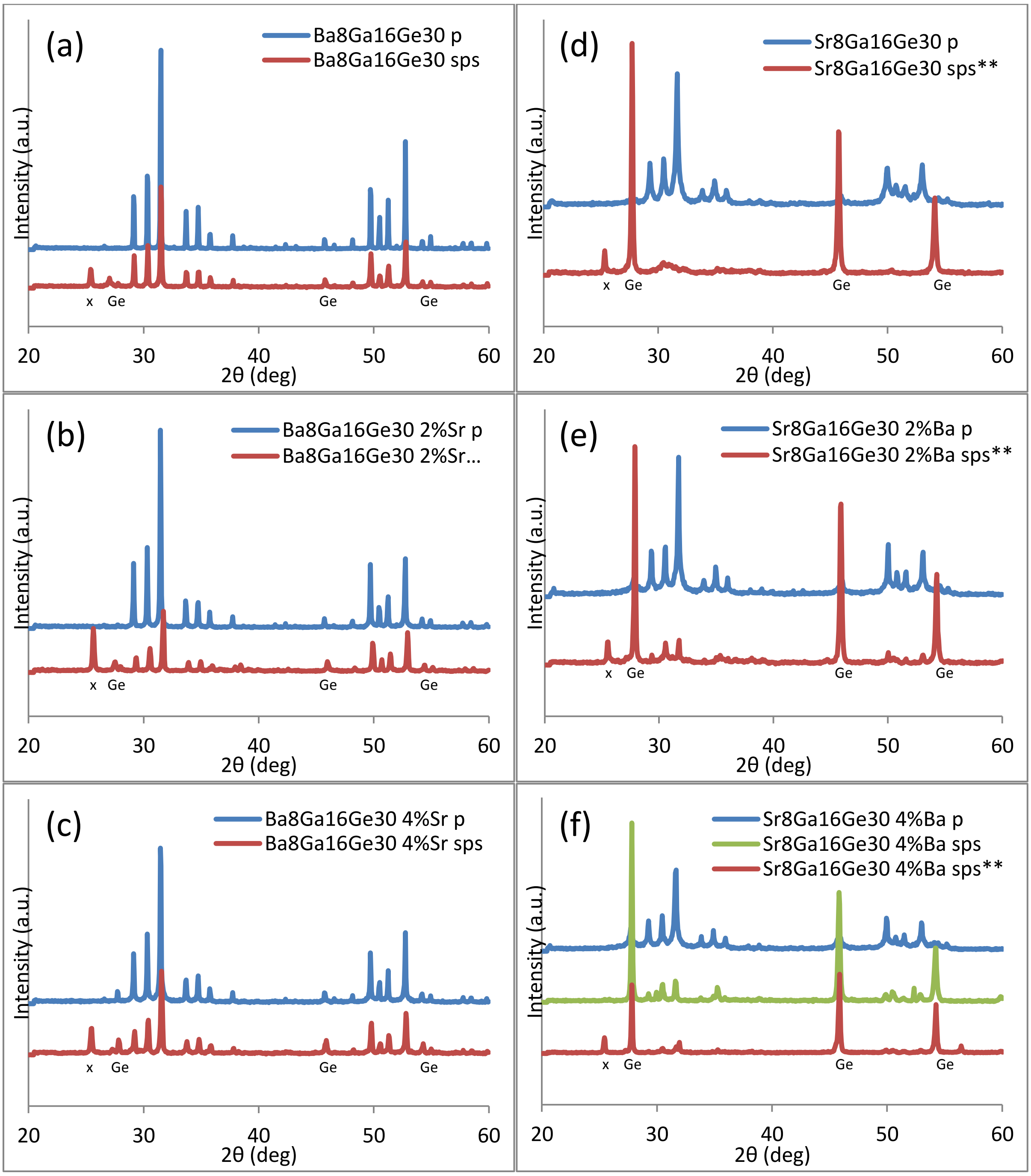

Figure 10. X-ray diffractorgrams for prepared samples of (BaSr)$_8$Ga$_{16}$Ge$_{30}$ in different composition ratios of Ba/Sr. For figures a) – f) marked with “p” denotes diffraction data collected from powders before spark plasma sintering while “sps” denotes diffraction data collected from polished surfaces of pellets. For figures d) – f) samples marked with “” are pellets after heat treatement for removal of Ga. Peaks position for impurity phases of germanium are marked with Ge. The peak in each figure marked with “x” mostly represents carbon (graphite) but also traces of Ba.**

The properties for the $Ba_8Ga_{16}Ge_{30}$ based compounds are shown in Figure 11. The electrical resistivity, Figure 11 (a), is for $Ba_8Ga_{16}Ge_{30}$ measured to be as lowest ca 30 mΩcm, which is at least a factor 10 higher than for $Ba_8Ga_{16}Ge_{30}$ reported in references that show values around 0.1 mΩcm [26], 1 mΩcm [20] [42] and 2 mΩcm [33]. In addition, the measured values show decreasing resistivity with increasing temperature, which is the opposite to the trend of increasing resistivity with temperature shown in the same references. In addition $Ba_8Ga_{16}Ge_{30}$ 4%Sr has a much steeper decrease at lower temperature than $Ba_8Ga_{16}Ge_{30}$ and $Ba_8Ga_{16}Ge_{30}$ 2%Sr. However the results show that the resistivities for the compounds are lowest at 450 °C with values of ca 30 mΩcm for $Ba_8Ga_{16}Ge_{30}$, 6 mΩcm for $Ba_8Ga_{16}Ge_{30}$ 2%Sr and 23 mΩcm for $Ba_8Ga_{16}Ge_{30}$ 4%Sr, but these values have not necessarily reached minimum. The Seebeck coefficients, Figure 11 (b), are shown to be, in the measured temperature interval, at its largest -160 µV/K for $Ba_8Ga_{16}Ge_{30}$, a slight decrease to -148 µV/K for $Ba_8Ga_{16}Ge_{30}$ 2%Sr and increased to -197 µV/K for sample $Ba_8Ga_{16}Ge_{30}$ 4%Sr, at 450 °C. Values for $Ba_8Ga_{16}Ge_{30}$ sample and the general trend of increasing Seebeck coefficient with temperature within given range matches previously reported results from references [9] [20] [26] [33] [42] . The power factor α^2/ρ, Figure 11 (c), was calculated to be largest for all compounds at 450 °C with $Ba_8Ga_{16}Ge_{30}$ 2%Sr having the largest. The results from the thermal conductivity measurements are shown in Figure 11 (d) for the $Ba_8Ga_{16}Ge_{30}$ based compounds. The values are fairly constant at the temperature interval with a slight increase at 450 °C. The thermal conductivities measured for $Ba_8Ga_{16}Ge_{30}$, ca 1.5 W/mK, are slightly lower than previously reported results where the TPS method [33] and the laser flash method [20] [26] [42] were used. Thermal conductivity results were not obtained from sample $Ba_8Ga_{16}Ge_{30}$ 4%Sr since the sintered sample broke during measurement.

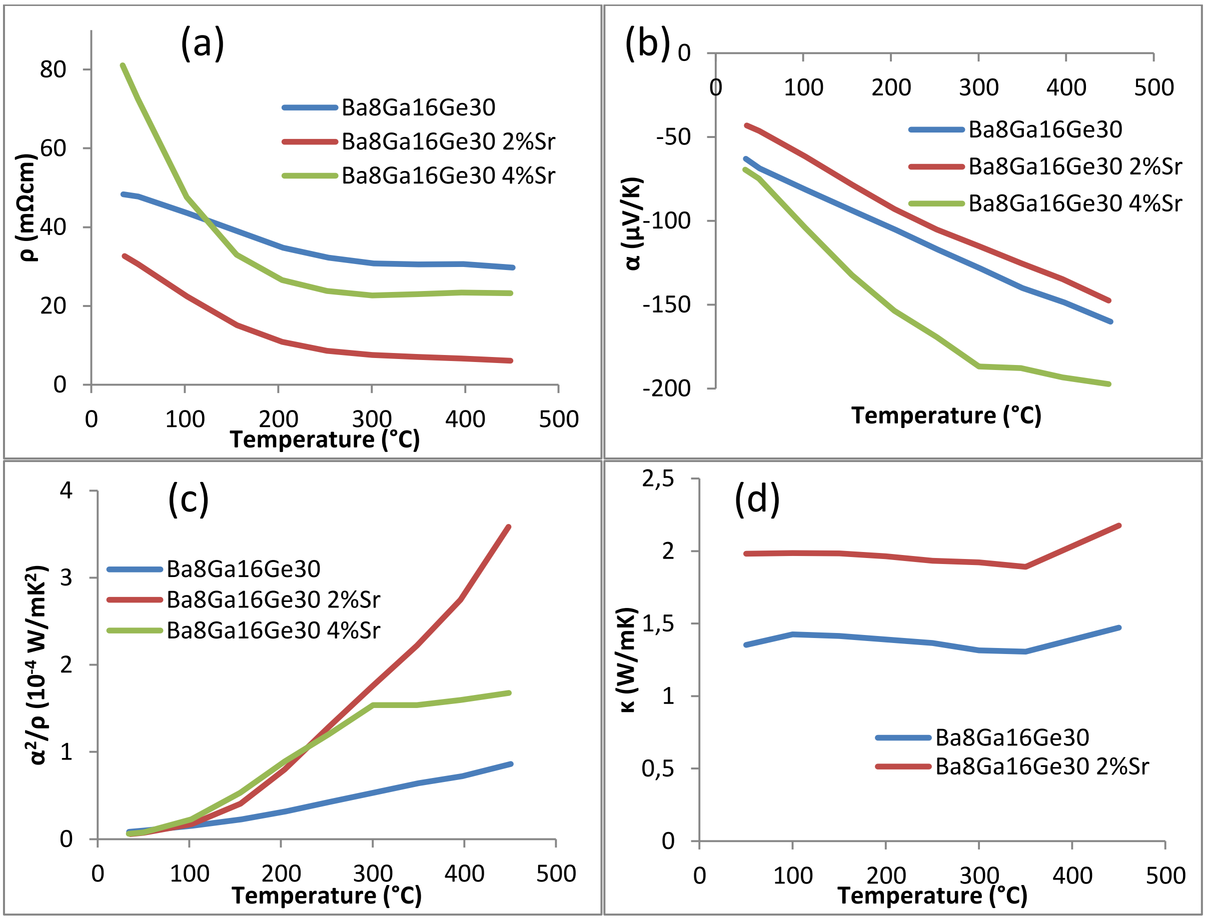

Figure 11. Measured properties as function of temperature for sintered samples of $Ba_8Ga_{16}Ge_{30}$, $Ba_8Ga_{16}Ge_{30}$ 2%Sr and $Ba_8Ga_{16}Ge_{30}$ 4%Sr. (a) Electrical resistivity. (b) Seebeck coefficient. (c) Power factor, α^2/ρ. (d) Thermal conductivity.

Properties for the $Sr_8Ga_{16}Ge_{30}$ based compounds are presented in Figure 12. The electrical resistivity, Figure 12 (a), was measured to be ca 0.5 mΩcm for $Sr_8Ga_{16}Ge_{30}$ and slightly lower for $Sr_8Ga_{16}Ge_{30}$ 2%Ba but an increased value for $Sr_8Ga_{16}Ge_{30}$ 4%Ba to ca 1.5 mΩcm. Values for sample $Sr_8Ga_{16}Ge_{30}$ and the small trend of increasing electrical resistivity with temperature are similar to that of previous reports [9] [19] [21]. The Seebeck coefficients, Figure 12 (b), are between 20 and 30 µV/K for both $Sr_8Ga_{16}Ge_{30}$ and $Sr_8Ga_{16}Ge_{30}$ 2%Ba but increase to ca 40 – 60 µV/K for $Sr_8Ga_{16}Ge_{30}$ 4%Ba, the positive numbers indicates that the compounds are p-doped. The values have a general increasing trend with temperature within the measured temperature range. These values are far lower than reported values of between -70 µV/K and -140 µV/K [9] [19] [21]. The power factor, Figure 12 (c), was the largest for $Sr_8Ga_{16}Ge_{30}$ 4%Ba. The thermal conductivity, Figure 12 (d), was ca 7 W/mK for $Sr_8Ga_{16}Ge_{30}$, increased to ca 8 W/mK for $Sr_8Ga_{16}Ge_{30}$ 2%Ba and decreased to ca 5 - 6 W/mK for $Sr_8Ga_{16}Ge_{30}$ 4%Ba. For the compounds the thermal conductivity decreases slightly to 350 °C to increase after that up to 450 °C. However the results have values much larger than reported in references of around 2 W/mK [19] and ca 1.5 W/mK [21] in the same temperature range.

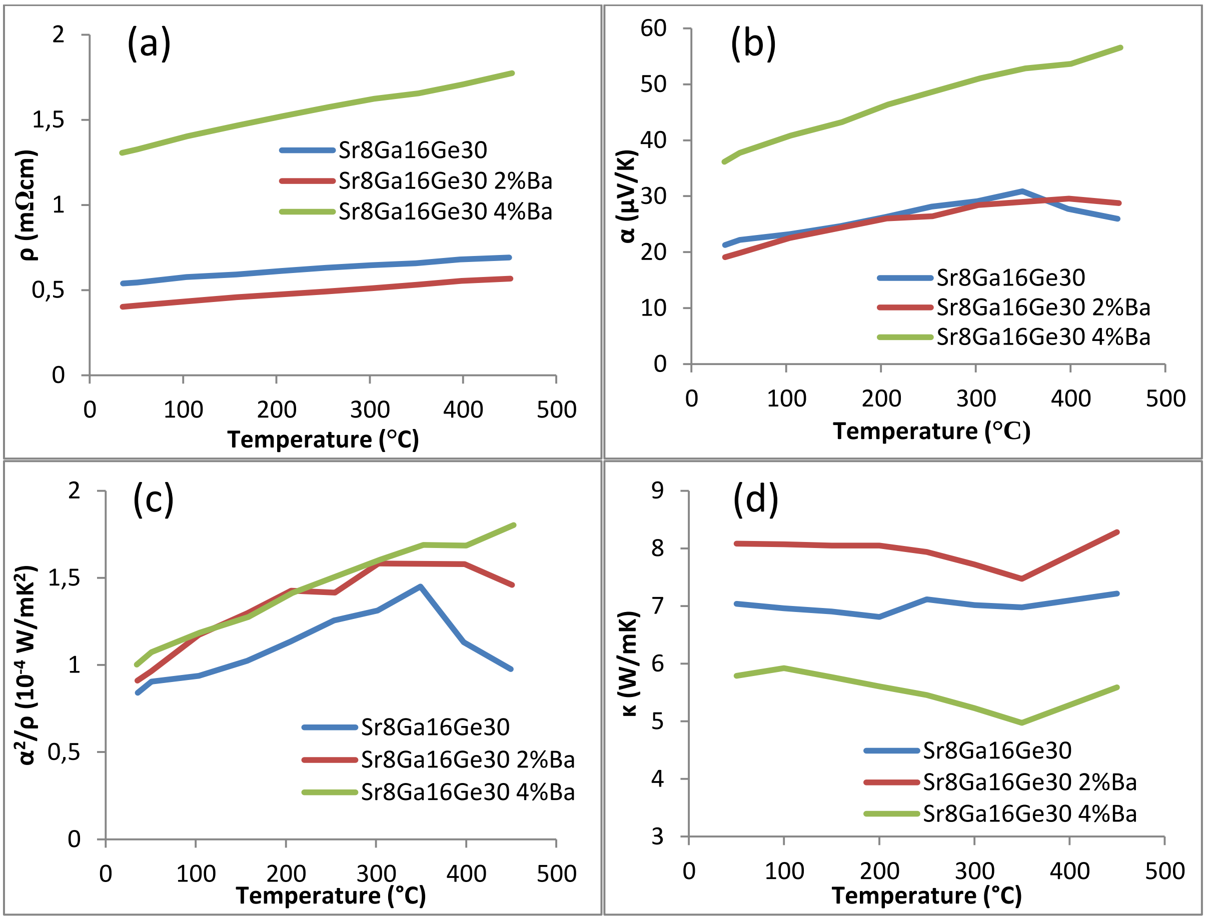

Figure 12. Measured properties as function of temperature for sintered samples of $Sr_8Ga_{16}Ge_{30}$, $Sr_8Ga_{16}Ge_{30}$ 2%Ba and $Sr_8Ga_{16}Ge_{30}$ 4%Ba. (a) Electrical resistivity. (b) Seebeck coefficient. (c) Power factor, α^2/ρ. (d) Thermal conductivity.

The dimensionless figures of merit are presented in Figure 13 and show a highest value of 0.026 for $Ba_8Ga_{16}Ge_{30}$ and increased to 0.074 for $Ba_8Ga_{16}Ge_{30}$ 2%Sr at 450 °C, in Figure 13 (a). In Figure 13 (b) the figure of merit is for $Sr_8Ga_{16}Ge_{30}$ largest 0.0073 at 350 °C while values for $Sr_8Ga_{16}Ge_{30}$ 2%Ba are slightly higher reach a largest value of 0.0079 at 450 °C. $Sr_8Ga_{16}Ge_{30}$ 4%Ba obtained the highest values of 0.0145 at 450 °C. However, all values are significantly lower than previously reported up to between ca 0.35 and 0.7 for $Ba_8Ga_{16}Ge_{30}$ [20] [26] [33] [42] and between ca 0.3 and 0.5 for $Sr_8Ga_{16}Ge_{30}$ [19] [21] at around 450 °C.

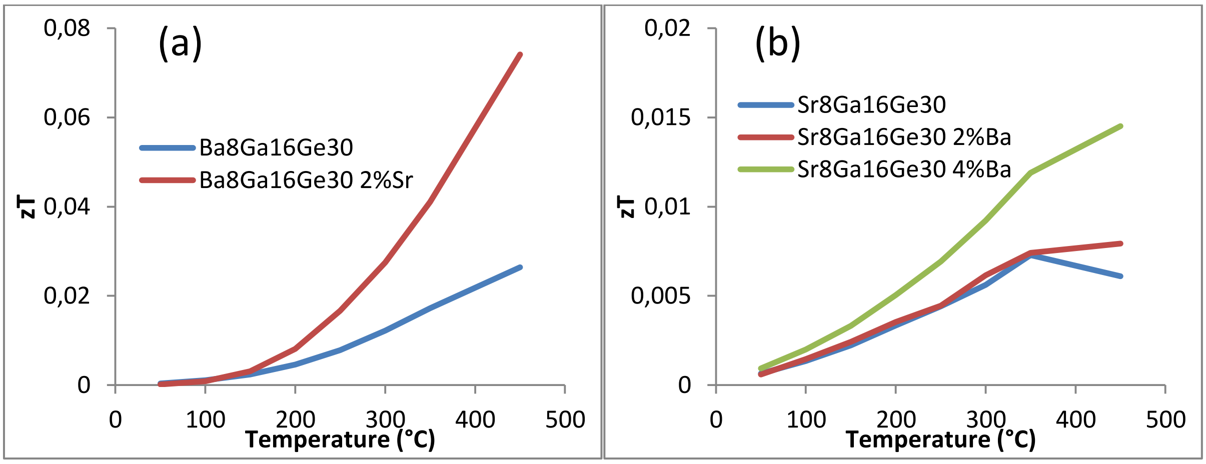

Figure 13. Dimensionless figure of merit as function of temperature for (a) $Ba_8Ga_{16}Ge_{30}$ and $Ba_8Ga_{16}Ge_{30}$ 2%Sr, (b) $Sr_8Ga_{16}Ge_{30}$, $Sr_8Ga_{16}Ge_{30}$ 2%Ba and $Sr_8Ga_{16}Ge_{30}$ 4%Ba.

5. Discussion

The XRD results showed that all samples had changed after the sintering, with appearance of other non-clathrate structure content. This could indicate that the synthesised samples were not stable enough to withstand the high temperature and pressure applied during sintering or alternatively that the samples had not fully reacted.

For the $Ba_8Ga_{16}Sn_{30}$ it shows clearly that the single crystal samples had higher thermoelectric properties in comparison to the sintered sample. The increased amount of tin in the sintered sample probably disturbed the measurements and lowered the overall thermoelectric properties which could be a result from the sintering process as the sintering parameters like time, temperature and pressure were likely not optimal.

The $Ba_8Ga_{16}Ge_{30}$ samples show only traces of impurity phases from the XRD results which indicate that the sintering did not alter the structure much, however the cracks found in the sintered samples suggest a non-optimal preparation of the samples. The increased electrical resistivity and lowered Seebeck coefficient for the $Ba_8Ga_{16}Ge_{30}$ samples were probably caused by imperfections in the material since the same instrument and settings were used for all samples. In comparison, $Ba_8Ga_{16}Ge_{30}$ contained the largest concentration of the clathrate structure, then $Ba_8Ga_{16}Ge_{30}$ 4%Sr and $Ba_8Ga_{16}Ge_{30}$ 2%Sr with somewhat lower concentrations from the appearance of the diffractograms. $Ba_8Ga_{16}Ge_{30}$ 2%Sr has lower electrical resistivity but higher thermal conductivity than $Ba_8Ga_{16}Ge_{30}$ which could be explained by that an increased electrical resistivity equals a lower electrical conductivity, which by Wiedemann-Franz law means a lower electronic thermal conductivity thus a lower total thermal conductivity. Despite the strange trend of the electrical resistivity curve for $Ba_8Ga_{16}Ge_{30}$ 4%Sr, it showed the highest Seebeck coefficient and a power factor between those of $Ba_8Ga_{16}Ge_{30}$ and $Ba_8Ga_{16}Ge_{30}$ 2%Sr but unfortunately no thermal conductivity was measured. $Ba_8Ga_{16}Ge_{30}$ 2%Sr showed overall strongest thermoelectric property with largest figure of merit.

For the $Sr_8Ga_{16}Ge_{30}$ samples the clathrate structures after sintering had greatly decreased and been replaced by Ge shown in the XRD and Ga that leaked during measurements. The synthesis route for the Sr clathrate compounds that were determined by modifying the synthesis route for Ba clathrate [33] had not been tried out before. However there have been reported similar attempts to synthesise Ge clathrate with mixed both Ba and Sr [43] [44] although with different compositions and under different conditions. The synthesis from stoichiometric ratios were supposed to give n-doped clathrates, but the $Sr_8Ga_{16}Ge_{30}$ samples turned out to be p-doped, which could be resulting from either the synthesis itself, the sintering or perhaps the heat treatment. The high content of Ge and Ga could also be the reason of the lowered electrical resistivity and increased thermal conductivity for the samples. When comparing the compounds, $Sr_8Ga_{16}Ge_{30}$ 2%Ba seems to have higher content of clathrate structure than $Sr_8Ga_{16}Ge_{30}$ 4%Ba and that $Sr_8Ga_{16}Ge_{30}$ has very little which could possibly describe why $Sr_8Ga_{16}Ge_{30}$ 2%Ba has the lowest electrical resistivity, but at the same time the electrical resistivity is only slightly higher for $Sr_8Ga_{16}Ge_{30}$ and further increased for $Sr_8Ga_{16}Ge_{30}$ 4%Ba. Apart from the high values of the thermal conductivities, it is fairly reasonable that $Sr_8Ga_{16}Ge_{30}$ 2%Ba has the highest value, $Sr_8Ga_{16}Ge_{30}$ little lower and $Sr_8Ga_{16}Ge_{30}$ 4%Ba even lower, this because higher electrical resistivity gives slightly lower thermal conductivity. Generally $Sr_8Ga_{16}Ge_{30}$ 4%Ba has the highest figure of merit and $Sr_8Ga_{16}Ge_{30}$ and $Sr_8Ga_{16}Ge_{30}$ 2%Ba has almost the same just slightly lower.

6. Conclusion

$Ba_8Ga_{16}Sn_{30}$ has been synthesised with tin flux method, electrical resistivity and Seebeck coefficient has been measured for a single crystal sample to around 7.5 mΩcm and -240 µV/K, respectively at ca 250 °C, which are in the same magnitude and temperature interval as previously reported. From spark plasma sintered sample the electrical resistivity was somewhat lower and the Seebeck coefficient greatly reduced indicating that the material might not be stable enough for sintering.

The synthesised samples of $Ba_8Ga_{16}Ge_{30}$ with substituted Sr showed a slight increase of figure of merit for $Ba_8Ga_{16}Ge_{30}$ with 2% substitution compared to pure $Ba_8Ga_{16}Ge_{30}$, however the measured electrical resistivity was a magnitude higher for the samples than reported values, which probably depends on flaws in the materials.

The $Sr_8Ga_{16}Ge_{30}$ samples with substituted Ba showed overall flaws during preparation and measurements like the large amounts of germanium phase in the XRD results and the leakage of gallium during measurements. Nevertheless the substitution of Ba seems to show small trend of increased figure of merit from pure $Sr_8Ga_{16}Ge_{30}$, $Sr_8Ga_{16}Ge_{30}$ with 2%Ba substituted to $Ba_8Ga_{16}Ge_{30}$ with 4%Ba substituted.

7. Future work

It would be interesting to further investigate and find a synthesis route for growing large single crystals of $Ba_8Ga_{16}Sn_{30}$ with the means available, since these show great potential for having good thermoelectric properties.

Synthesise $Ba_8Ga_{16}Ge_{30}$ with Sr substitutions using a more finely tuned and controlled synthesis and sample preparation to make flawless samples to further investigate the effects on the properties from the substitution.

Search for possible synthesis routes for the $Sr_8Ga_{16}Ge_{30}$ compounds and investigate their stability.

If possible, for all the different compounds, also study the composition of the synthesised materials, determine and verify the structures with other methods than X-ray diffraction.

Acknowledgements

I would like to thank Professor Anders Palmqvist for introducing me to nanomaterials chemistry, giving me the opportunity to work in his group and for all the guidance from the beginning to the completion of this interesting project.

I would also give my thanks to my supervisor Richard Heijl for all the guidance throughout the project, giving me knowledge and practical advice for working in this research environment and all the support and feedback through the thesis.

Further, I am thankful for the help with the spark plasma sintering given by Kasper Borup and his supervisor Bo Brummerstedt Iversen for giving access to the instruments, at the Department of Chemistry at Aarhus University Denmark.

Finally, I give my gratitude to the MISTRA E4 program for financing this project.

References

1. Rowe, D.M., *Thermoelectric Handbook Macro to Nano*. 2005, Boca Raton: CRC Press.
2. Goldsmid, H.J., *Chapter 3 Conversion Efficiency and Figure-of-Merit*, in *CRC Handbook of Thermoelectrics*. 1995, CRC Press: Boca Raton.
3. Snyder, G.J. and E.S. Toberer, *Complex thermoelectric materials.* Nature Materials, 2008. **7**: p. 105-114.
4. Rowe, D.M., *CRC Handbook of Thermoelectrics*. 1995, Boca Raton: CRC Press.
5. Matsubara, K. and M. Matsuura, *Chapter 52 A Thermoelectric Application to Vehicles*, in *Thermoelectric Handbook Macro to Nano*. 2005, CRC Press: Boca Raton.
6. Nolas, G.S., et al., *Semiconducting Ge clathrates: Promising candidates for thermoelectric applications.* Applied Physics Letters, 1998. **73**(2): p. 178-180.
7. Kittel, C., *Introduction to Solid State Physics*. 2005: Wiley.
8. Vaqueiro, P. and A.V. Powell, *Recent developments in nanostructured materials for high-performance thermoelectrics.* Journal of Materials Chemistry, 2010. **20**: p. 9577-9584.
9. Kuznetsov, V.L., et al., *Preaparaton and thermoelectric properties of A8IIB16IIIB30IV clathrate compounds.* Journal of Applied Physics, 2000. **87**(11): p. 7871-7875.
10. Christensen, M., S. Johnsen, and B.B. Iversen, *Thermoelectric clathrates of type I.* Dalton Transactions, 2010. **39**: p. 978-992.
11. Paschen, S., et al., *Structural, transport, magnetic, and thermal properties of Eu8Ga16Ge30.* Physical Review B, 2001. **64**: p. 214404.
12. Avila, M.A., et al., *Glasslike verusus crystalline thermal conductivity in carrier-tuned Ba8Ga16X30 clathrates (X=Ge,Sn).* Physical Review B, 2006. **74**: p. 125109.
13. Ma, Y., R. Heijl, and A.E.C. Palmqvist, *Composite thermoelectric materials with embedded nanoparticles.* Journal of Materials Science, 2013. **48**: p. 2767-2778.
14. Bux, S.K., J.-P. Fleurial, and R.B. Kaner, *Nanostructure materials for thermoelectric applications.* Chemical Communications, 2010. **46**: p. 8311-8324.
15. Datta, A., et al., *Chapter 14. The Bottom-Up Approach to Bulk Thermoelectric Materials with Nanoscale Domains*, in *Thermoelectrics And Its Energy Harvesting: Materials, Preparation, and Characterization in Thermoelectrics*. 2012, CRC Press: Boca Raton.
16. Smart, L.E. and E.A. Moore, *Solid State Chemistry An Introduction*. 2005, Boca Raton: CRC Press.
17. Deng, S.K., et al., *Enhancement of thermoelectric efficiency in type-VIII clathrate Ba8Ga16Ge30 by Al substitution for Ga.* 2010. **108**: p. 073705.
18. Wang, H.F., et al., *Synthesis and thermoelectric properties of single crystalline and polycrystalline Ba8Ga16Ge30.* Journal of Alloys and Compounds, 2010. **491**: p. 684-688.
19. Fujita, I., et al., *Thermoelectric properties of sintered clathrate compounds Sr8GaxGe46−x with varoius carrier concentrations.* Journal of Applied Physics, 2006. **99**: p. 093707.
20. Hou, X., et al., *Growth and thermoelectric properties of Ba8Ga16Ge30 clathrate crystals.* Journal of Alloys and Compounds, 2009. **482**: p. 544-547.
21. Cao, W.-Q., et al., *The effects of In isoelectronic substitution for Ga on the thermoelectric properties of Sr8Ga16−xInxGe30 type-I clathrates.* Journal of Physics D: Applied Physics, 2008. **41**: p. 215105.
22. Bentien, A., et al., *Crystal structures, atomic vibrations, and disorder of the type-I thermoelectric clathrates Ba8Ga16Si30, Ba8Ga16Ge30, Ba8In16Ge30, and Sr8Ga16Ge30.* Physical Review B, 2005. **71**: p. 144107.
23. Bentien, A., et al., *Experimental Charge Densities of Semiconducting Cage Structures Containing Alkaline Earth Guest Atoms.* Angewandte Chemie International Edition, 2000. **39**(20): p. 3613-3616.
24. Bryan, J.D., et al., *Nonstoichiometry and chemical purity effect in the thermoelectric Ba8Ga16Ge30 clathrate.* Journal of Applied Physics, 2002. **92**(12): p. 7281.

25. Christensen, M., et al., *Crystal Structures of Thermoelectric n- and p-type Ba8Ga16Ge30 Studies by Single Crystal, Multitemperature, Neutron Diffraction, Conventional X-ray Diffraction and Resonant Synchotron X-ray Diffraction.* Journal of American Chemical Society, 2006. **128**(49): p. 15657.
26. Okamoto, N.L., et al., *Effect of In additions on the thermoelectric properties of the type-I clathrate compound Ba8Ga16Ge30.* Journal of Applied Physics, 2007. **101**: p. 113525.
27. Martin, J., et al., *Structural and transport properties of Ba8Ga16SixGe30−x clathrates.* Journal of Applied Physics, 2006. **99**: p. 044903.
28. Eisenmann, B., H. Schäfer, and R. Zagler, *Die Verbindungen A8IIB16IIIB30IV (AII=Sr,Ba; BIII=Al, Ga; BIV=Si,Ge,Sn) Und Ihre Käfigstrukturen.* Journal of the Less-Common Metals, 1986. **118**: p. 43-55.
29. Bryan, J.D., et al., *Superconductivity in germanium clathrate Ba8G16Ge30.* Physical Review B, 1999. **60**(5): p. 3064-3067.
30. Zhang, Y., et al., *Gallium distribution in the clathrates Sr8Ga16Ge30 and Sr4Eu4Ga16Ge30 by resonant diffraction.* Applied Physics Letters, 2002. **80**(16): p. 2931-2933.
31. Mudryk, Y., et al., *Thermoelectricity of clathrate I Si and Ge phases.* Journal of Physics: Condensed Matter, 2002. **14**: p. 7991-8004.
32. Christensen, M. and B.B. Iversen, *Host Structure Engineering in Thermoelectric Clathrates.* Chemistry of Materials, 2007. **19**: p. 4896-4905.
33. Heijl, R., et al., *Thermoelectric properties of Ba8Ga16Ge30 with TiO2 nanoinclusions.* Journal of Applied physics, 2012. **112**: p. 044313.
34. Gustafsson, S.E., *Transient plane source techniques for thermal conductivity and thermal diffusivity measurements of solid materials.* Review of Scientific Instruments, 1991. **62**: p. 797-804.
35. Burkov, A.T., *Chapter 22. Measurements of Resistivity and Thermopower: Principles and Practical Realization*, in *Thermoelectric Handbook Macro to Nano*. 2005, CRC Press: Boca Raton.
36. Tritt, T.M., *Chapter 23. Electrical and Thermal Tranposrt Measurement Techniques for Evaluation of the Figure-of-Merit of Bulk Thermoelectric Materials*, in *Thermoelectric Handbook Macro to Nano*. 2005, CRC Press: Boca Raton.
37. *ULVAC Technologies, Inc.* [Online] 2012 December; Available from: http://www.ulvac.com/thermal/zem%203.asp.
38. *CCR Process Products*. [Online] 2012 December; Available from: http://www.ccrprocessproducts.com/zem-3-ulvac-seebeck-coefficient-electric-resistance-measuring-system-ulvac.html.
39. Huo, D., et al., *Structural, transport, and thermal properties of the single-crystalline type-VIII clathrate Ba8Ga16Sn30.* Physical Review B, 2005. **71**: p. 075113.
40. Deng, S.K., et al., *Sn-based type-VIII single-crystal clathrates with large figure of merit.* Chinese Physics B, 2012. **21**(1): p. 017401.
41. Saiga, Y., et al., *Thermoelectric properties of type-VIII clathrate Ba8Ga16Sn30 doped with Cu.* Journal of Alloys and Compounds, 2012. **537**: p. 303-307.
42. Saramat, A., et al., *Large thermoelectric figure of merit at high temperature in Czochralski-grown clathrate Ba8Ga16Ge30.* Journal of Applied Physics, 2006. **99**: p. 023708.
43. Cai, K.F., et al., *Preparation and Characterization of Ba8Ga16Ge30/Sr8Ga16Ge30 Core-Shell Single Crystals.* Crystal Growth & Design, 2006. **6**(8): p. 1797-1800.
44. Wang, L., et al., *Synthesis and Transport Properties of Polycrystalline Co-filled Type-I Clathrate Compound (Sr,Ba)8Ga16Ge30.* Materials Science Forum, 2009. **610-613**: p. 441-445.

Appendix A – Synthesis

In this appendix the protocols with details of the synthesis are presented for the synthesised compounds.

The materials used were:

- Ba – Barium, dendritic pieces 99.99% from Sigma-Aldrich
- Ga – Gallium, liquid 99.9995% from Sigma-Aldrich
- Ge – Germanium, chips 99.999% from Sigma-Aldrich
- Sn – Tin, 3mm shots 99.999% from Alfa Aesar
- Sr – Strontium, dendritic pieces 99.99% from Sigma-Aldrich

A1. $Ba_8Ga_{16}Sn_{30}$

Four batches of $Ba_8Ga_{16}Sn_{30}$ were made with some variations in the starting material composition and heating program.

A1.1. $Ba_8Ga_{16}Sn_{30}$ batch 1

The first batch of the compound $Ba_8Ga_{16}Sn_{30}$ was prepared in an argon filled glove box by mixing 2.010 g Ba, 2.05319 g of Ga and 10.967 g of Sn into an alumina crucible. The crucible was then put into a quartz tube, sealed, evacuated and put into a tube furnace. It was heated to 490 °C over 10 h and dwelled for 10 h, cooled to 390 °C over 50 h and cooled to 25 °C over 8 h.

The sample was hammered out of the crucible that was broken and it was one inhomogeneous piece with small shiny crystals in it with the top surface of greyish colour compared to the surfaces that were attached to the crucible and the newly cleaved surfaces that had a silvery colour.

The samples the top greyish layer was removed by sandpapering and then put together with some powder used for XRD and treated in the furnace again. The same heating program was used as the first time but with cooling time 80 h from 490 °C to 390 °C.

The result was a large piece not stuck in the crucible, and the powder was still there around it. When cleaved, there was a shiny homogeneous relatively large piece of crystal with defined boundaries between crystal and surrounding excess tin.

A1.2. $Ba_8Ga_{16}Sn_{30}$ batch 2

Second synthesis batch of $Ba_8Ga_{16}Sn_{30}$ was made with more tin flux, the ratio of starting material for Ba:Ga:Sn was 8:16:60 and was prepared in a glove box where 2.588 g Ba, 2.591 g Ga and 16.787 g Sn were mixed in an alumina crucible sealed in a quartz tube. The tube was evacuated and put in tube furnace heated to 490 °C over 10 h then dwelled for 10 h, cooled to 390 °C over 100 h and cooled to 25 °C over 8 h.

The product from the second synthesis was similar to the first synthesis after the first run in the furnace but with fewer shiny crystals visible. Also the crucible was broken and some powder and a drop of sample were outside the crucible in the bottom of the quartz tube.

This sample was prepared for further synthesis by first removing the top dark grey layer with sandpaper and then cut the sample into smaller pieces (ca 2 - 3 mm diameter) as far as possible into a crucible. More starting material was added to the same batch, (2.590 g Ba, 2.661 g Ga and 16.845 g Sn) where the dendritic Ba was cut to smaller pieces. The same heating program as before was used.

The results showed grainy and dark grey sample that was stuck to the crucible. When the sample was hammered out of the crucible it showed that it contained air bubbles and that the compounds were not well mixed. From the samples that were separated from the crucible, some were in powder form and other of ca two millimetre large irregularly shaped pieces. Everything was dark grey and had many small glimmering parts and some small parts were gold/yellow.

The sample was once again prepared for synthesis using a heating program that was chosen to be different than previously. The material was heated to 690 °C over 14 h, dwelled for 10 h, first cooled to 490 °C over 8 h then to 390 °C over 100 h and finally to 25 °C over 8 h.

The sample taken out was on the top layer all grainy and dark coloured (like before), this layer was rather loose and easily removed. The rest was hard to hammer out, all was stuck in the crucible, it was heated on a heat plate to ca 250 °C. Lot of grainy pieces could be scraped off with a spatula, the sample was all grainy and porous with small air bubbles, and this was light silver grey coloured. When reached the bottom layer that was too hard to scrape, the sample was heated further and then the rest was removed with more force. This was in large pieces, dense and no air bubbles.

A1.3. $Ba_8Ga_{16}Sn_{30}$ batch 3

Starting ratio was 8:16:50 of Ba:Ga:Sn with weighed material: 3.370 g Ba, 3.422 g Ga and 18.27 g Sn. The batch of 25 g of starting material would theoretically give 17.7 g of $Ba_8Ga_{16}Sn_{30}$, if grown to one single crystal, enough for measurement with Hot Disk and ZEM-3. Due to the unsuccessful previous synthesis, new heating program was tried out, (modified synthesis of that used in references *Huo et al. Structural, transport, and thermal properties of the single-crystalline type-VIII clathrate* $Ba_8Ga_{16}Sn_{30}$ *2005 and Deng et al. Enhancement of thermoelectric efficiency in type-VIII clathrate* $Ba_8Ga_{16}Sn_{30}$ *by Al Substitution for Ga 2010).* The materials were heated to 950 °C over 10 h and dwelled for 2 h, cooled to 490 °C over 6 h, cooled to 460 °C over 13 h, cooled to 390 °C over 60 h and cooled to 25 °C over 4 h.

The results were visible that everything had melted and solidified with a flat surface and the crucible was all intact. It was all stuck in the crucible and the content was melted out and then the top surface turned dark grey. The sample was otherwise light silver and contained visible small 1 - 2 mm crystals.

The sample batch was prepared and put back in furnace again, heated to 590 °C over 6 h, dwelled for 2 h, cooled to 490 °C over 2 h, cooled to 390 °C over 80 h and cooled to 25 °C over 4 h.

The results were defined crystals mostly with diameter about 1 - 2 mm but some had diameter up to ca 4 mm. The top surface was dark grey and the sample was stuck in the crucible but the pieces on top were not all melted together completely but they were in one chunk.

A1.4. $Ba_8Ga_{16}Sn_{30}$ batch 4

Starting ration of 8:16:50 of Ba:Ga:Sn with 3.370 g Ba, 3.436 g Ga and 18.207 g Sn weighed. Heated to 950 °C over 10 h, dwelled for 10 h, cooled to 500 °C over 10 h and dwelled for 10 h, cooled to 390 °C over 120 h and to 25 °C over 4 h.

The sample taken out showed large chunks with some tiny regular shaped crystals and some grainy parts. Later on, this batch was put in a crucible together with a small $Ba_8Ga_{16}Ge_{30}$ seed, very thin and approximately smaller than 2 x 2mm, and heated to 490 °C over 10 h, dwelled for 10 h, cooled to 390 °C over 80 h and to 25 °C over 8 h (same as batch 1, second heat treatment cycle).

Large chunks were loosely-stuck in each other, looked like they had not completely melted together, and they were not very stuck in the crucible, all over dark and ashy colour. One piece cleaved and showed light silver lustre.

A2. $(BaSr)_8Ga_{16}Ge_{30}$

Six samples of $(BaSr)_8Ga_{16}Ge_{30}$ were synthesised, they were $Ba_8Ga_{16}Ge_{30}$, $Ba_8Ga_{16}Ge_{30}$ with 2%Sr and 4%Sr substitution, respectively, and $Sr_8Ga_{16}Ge_{30}$, $Sr_8Ga_{16}Ge_{30}$ with 2%Ba and 4%Ba substitution, respectively.

A2.1. $Ba_8Ga_{16}Ge_{30}$

The $Ba_8Ga_{16}Ge_{30}$ batches were prepared with stoichiometric ratios and an addition of 2.5% Ba. One batch was prepared from 3.057 g Ba, 3.021 g Ga and 5.915 g Ge and heated to 1050 °C over 8 h, dwelled for 1 h, cooled to 980 °C over 4 h then to 963 °C and dwelled for 36 h, cooled to 930 °C over 4 h and to 20 °C over 9 h.

The sample was dark grey coloured and taken out from crucible. The cleaved surfaces were not as even as previously synthesised $Ba_8Ga_{16}Ge_{30}$ and also overall somewhat darker in colour. This batch was treated in the same way as the second synthesis of $Ba_8Ga_{16}Sn_{30}$ batch 4. Heated to 490 °C over 10 h, dwelled for 10 h, cooled to 390 °C over 80 h and to 25 °C over 8 h.

A second batch of $Ba_8Ga_{16}Ge_{30}$ was synthesised from 3.057 g Ba, 3.027 g Ga and 5.915 g Ge, heated to 1050 °C over 8 h, dwelled for 1 h, cooled to 980 °C over 4 h, cooled to 963 °C over 12 h and dwelled for 36 h, cooled to 930 °C over 14 h and to 20 °C over 13 h.

The sample was easily removed from the crucible in one single piece having rather smooth surface and a couple air bubbles on the bottom side.

These two batches of $Ba_8Ga_{16}Ge_{30}$ were mixed together with two previously synthesised batches of $Ba_8Ga_{16}Ge_{30}$ to form the spark plasma sintered $Ba_8Ga_{16}Ge_{30}$ sample in the sample preparation part.

A2.2. $Ba_8Ga_{16}Ge_{30}$ 2%Sr

The starting materials were in stoichiometric ratio, 2.946 g Ba, 0.039 g Sr, 3.050 g Ga and 5.965 g Ge were weighed and heated to 1050 °C over 8 h, dwelled for 1 h, cooled to 980 °C over 4 h, cooled to 963 °C over 6 h and dwelled for 36 h, cooled to 930 °C over 4 h, cooled to 780 °C over 14 h, cooled to 730 °C over 12 h and cooled to 20 °C over 4 h.

The sample was not stuck in the crucible and easily removed but had many air bubbles on the bottom side. The top side looked like a darker thin layer with some surface cracks that reveal lighter silver colour beneath.

A2.3. $Ba_8Ga_{16}Ge_{30}$ 4%Sr

Starting material of 2.892 g Ba, 0.077 g Sr, 3.058 g Ga and 5.975 g Ge was weighed and heated to 1050 °C over 8 h, dwelled for 1 h, cooled to 980 °C over 4 h, cooled to 963 °C over 4 h and dwelled for 30 h, cooled to 930 °C over 4 h, cooled to 780 °C over 6 h, cooled to 730 °C over 8 h and cooled to 20 °C over 4 h.

The crucible was cracked having a small lump on the outside at one of the cracks which turned into some red/orange and black-ashy metal coloured powder after about 2 hours. One day later some of it showed yellow colour powder also. Inside the crucible, the sample itself was not spread over all the bottom of the crucible and was very hard to hammer out and it had a “metallic smell”.

This sample was further heat treated (for annealing). It was heated to 600 °C over 4 h, dwelled for 42 h and cooled to 20 °C over 2 h.

A2.4. $Sr_8Ga_{16}Ge_{30}$ 4%Ba

The following starting material was weighed: 0.132 g Ba, 2.013 g Sr, 3.338 g Ga and 6.519 g Ge and heated to 1050 °C over 8 h, dwelled for 2 h, cooled to 963 °C over 8 h, dwelled for 4 h, cooled to 930 °C over 4 h, cooled to 780 °C over 10 h, cooled to 730 °C over 30 h and cooled to 20 °C over 4 h.

The synthesised material in the crucible was not evenly spread in the crucible bottom and was really hard to get all of it out from the crucible. This sample was heat treated again in the same way as for $Ba_8Ga_{16}Ge_{30}$ 4%Sr. It was heated to 600 °C over 4 h, dwelled for 42 h and cooled to 20 °C over 2 h.

A2.5. $Sr_8Ga_{16}Ge_{30}$ 2%Ba

A batch of 10 g starting material prepared from 0.055 g Ba, 1.716 g Sr, 2.778 g Ga and 5.444 g Ge was heated to 1050 °C over 8 h, dwelled for 2 h, cooled to 980 °C over 4 h, cooled to 930 °C over 5 h, dwelled for 12 h, cooled to 930 °C over 4 h, cooled to 780 °C over 10 h, dwelled for 10 h, cooled to 730 °C over 30 h and cooled to 20 °C over 4 h.

The sample was not evenly spread in the crucible and was hard and the newly cleaved surfaces hade metallic fine lustre.

A2.6. $Sr_8Ga_{16}Ge_{30}$

Starting material of 2.106 g Sr, 3.361 g Ga and 6.545 g Ge were heated to 1050 °C over 8 h, dwelled for 2 h, cooled to 780 °C over 12 h, dwelled for 10 h, cooled to 730 °C over 30 h, dwelled for 24 h and cooled to 20 °C over 3 h.

The sample had silver colour with metallic lustre but was hard.

Appendix B – Results

This section contains the measurement data for the different compounds and methods.

B1. $Ba_8Ga_{16}Sn_{30}$

Table 2. Electrical resistivity, Seebeck coefficient and powerfactor for $Ba_8Ga_{16}Sn_{30}$ single crystal sample.

Temperature (°C)	Electrical resistivity (mΩcm)	Seebeck coefficient (μV/K)	Powerfactor (10^{-4} W/mK^2)
32.69738	5.42947	-199.869	7.357524
49.57434	5.580894	-201.502	7.275332
102.4265	6.066822	-220.818	8.037232
165.8431	6.665691	-230.536	7.973187
204.4947	6.982164	-238.012	8.11351
243.3994	7.563162	-243.533	7.841711
306.3353	8.282831	-233.143	6.562455
358.9239	8.04463	-215.228	5.758252

Table 3. Electrical resistivity, Seebeck coefficient and powerfactor for $Ba_8Ga_{16}Sn_{30}$ spark plasma sintered sample.

Temperature (°C)	Electrical resistivity (mΩcm)	Seebeck coefficient (μV/K)	Powerfactor (10^{-4} W/mK^2)
34.89366	2.53478	-3.84403	0.00583
50.47486	2.645664	-4.6432	0.008149
103.8031	3.03903	-7.7141	0.019581
157.8	3.556644	-13.7979	0.053529
206.2725	5.360165	-23.8959	0.10653
254.7253	5.322788	-26.6095	0.133025
303.3275	5.156311	-27.9592	0.151604
351.3047	4.754746	-27.5865	0.160053

Table 4. Thermal conductivity for single crystal of $Ba_8Ga_{16}Sn_{30}$ from figure in reference Deng et al. 2010.

Temperature (°C)	Thermal conductivity (W/mK)
50	0.71
100	0.69
150	0.69
200	0.75
250	0.85
300	1.11
350	1.4

Table 5. Thermal conductivity for spark plasma sintered sample of $Ba_8Ga_{16}Sn_{30}$.

Temperature (°C)	Thermal conductivity (W/mK)
50	2.448428
100	2.536174
150	2.5779
200	2.563851
250	2.253429
300	2.373518
350	2.609877

Table 6. Figure of merit for $Ba_8Ga_{16}Sn_{30}$ spark plasma sintered sample.

Temperature (°C)	Figure of merit zT
50	0.014857
100	0.03169
150	0.046394
200	0.063292
250	0.086998
300	0.082946
350	0.077222

Table 7. Figure of merit for $Ba_8Ga_{16}Sn_{30}$ single crystal sample.

Temperature (°C)	Figure of merit zT
50	0.051235
100	0.116482
150	0.17333
200	0.21636
250	0.230639
300	0.177364
350	0.143956

B2. $(BaSr)_8Ga_{16}Ge_{30}$

Table 8. Electrical resistivity, Seebeck coefficient and powerfactor for $Ba_8Ga_{16}Ge_{30}$ spark plasma sintered sample.

Temperature (°C)	Electrical resistivity (mΩcm)	Seebeck coefficient (μV/K)	Powerfactor (10^{-4} W/mK^2)
34.33081	48.34361	-63.0112	0.082129
50.30392	47.734	-68.7491	0.099016
103.1962	43.55796	-81.5951	0.152848
156.9488	38.92619	-94.2116	0.228017
205.3722	34.78529	-105.444	0.319631
253.8609	32.20805	-117.216	0.426585
302.1888	30.80909	-128.512	0.536056
350.1285	30.50768	-140.07	0.643107
398.0278	30.62313	-148.732	0.722364
450.7688	29.74764	-160.152	0.862204

Table 9. Electrical resistivity, Seebeck coefficient and powerfactor for $Ba_8Ga_{16}Ge_{30}$ 2%Sr spark plasma sintered sample.

Temperature (°C)	Electrical resistivity (mΩcm)	Seebeck coefficient (μV/K)	Powerfactor (10^{-4} W/mK^2)
35.53607	32.6572	-43.188	0.057115
49.93064	30.61666	-46.4288	0.070407
102.3015	22.43787	-61.7767	0.170086
155.8413	15.11379	-78.4525	0.407231
204.0772	10.85453	-93.0515	0.797693
252.2249	8.610347	-105.236	1.286207
300.5231	7.514532	-115.075	1.762218
348.2116	7.070005	-125.251	2.218913
395.9164	6.619553	-134.798	2.74498
448.4123	6.073555	-147.537	3.58393

Table 10. Electrical resistivity, Seebeck coefficient and powerfactor for $Ba_8Ga_{16}Ge_{30}$ 4%Sr spark plasma sintered sample.

Temperature (°C)	Electrical resistivity (mΩcm)	Seebeck coefficient (μV/K)	Powerfactor (10^{-4} W/mK^2)
33.71573	81.08466	-69.624	0.059783
49.53856	72.64698	-74.8842	0.07719
102.0684	47.57546	-104.091	0.227741
155.6024	32.9391	-132.39	0.53211
204.0251	26.53786	-153.751	0.890774
252.1902	23.80085	-169.262	1.203724
300.5204	22.68199	-186.812	1.538609
348.3222	22.96741	-187.865	1.536671
396.0366	23.40346	-193.386	1.597977
448.5585	23.22082	-197.438	1.678737

Table 11. Thermal conductivity for $Ba_8Ga_{16}Ge_{30}$ and $Ba_8Ga_{16}Ge_{30}$ 2%Sr spark plasma sintered samples.

Temperature (°C)	Thermal conductivity (W/mK) $Ba_8Ga_{16}Ge_{30}$	Thermal conductivity (W/mK) $Ba_8Ga_{16}Ge_{30}$ 2%Sr
50	1.35328	1.982515
100	1.424348	1.984986
150	1.413401	1.982707
200	1.39058	1.963429
250	1.365562	1.93332
300	1.315668	1.920869
350	1.305548	1.891888
450	1.470943	2.176664

Table 12. Figure of merit for $Ba_8Ga_{16}Ge_{30}$ and $Ba_8Ga_{16}Ge_{30}$ 2%Sr spark plasma sintered samples.

Temperature (°C)	Figure of merit zT $Ba_8Ga_{16}Ge_{30}$	Figure of merit zT $Ba_8Ga_{16}Ge_{30}$ 2%Sr
50	0.000366	0.000178
100	0.001073	0.000857
150	0.00242	0.003081
200	0.004597	0.008126
250	0.00781	0.016632
300	0.012223	0.027522
350	0.017241	0.04105
450	0.026377	0.074094

Table 13. Electrical resistivity, Seebeck coefficient and powerfactor for $Sr_8Ga_{16}Ge_{30}$ spark plasma sintered sample.

Temperature (°C)	Electrical resistivity (mΩcm)	Seebeck coefficient (µV/K)	Powerfactor (10^{-4} W/mK^2)
35.46296	0.5389564	21.27884	0.840122
50.95398	0.544229	22.18853	0.904639
103.5302	0.5758129	23.23257	0.937374
157.0084	0.5922292	24.62907	1.02425
205.1225	0.6111341	26.32921	1.134329
253.2664	0.630923	28.14568	1.255588
301.5489	0.6458586	29.11898	1.31285
349.3223	0.6574896	30.88292	1.450601
397.0441	0.680423	27.72923	1.130047
449.487	0.6913532	25.99012	0.977049

Table 14. Electrical resistivity, Seebeck coefficient and powerfactor for $Sr_8Ga_{16}Ge_{30}$ 2%Ba spark plasma sintered sample.

Temperature (°C)	Electrical resistivity (mΩcm)	Seebeck coefficient (µV/K)	Powerfactor (10^{-4} W/mK^2)
35.32579	0.4013534	19.11617	0.910489
50.60447	0.4082353	19.83299	0.963531
103.6298	0.4329982	22.54046	1.173381
157.4303	0.4578736	24.38122	1.298271
205.9128	0.4757187	26.04568	1.426005
254.2466	0.4922199	26.39773	1.415708
302.6468	0.5110046	28.43603	1.582389
350.458	0.5309508	28.97327	1.581033
398.2003	0.5546918	29.58938	1.578411
450,7192	0,5673262	28,7736	1,459336

Table 15. Electrical resistivity, Seebeck coefficient and powerfactor for $Sr_8Ga_{16}Ge_{30}$ 4%Ba spark plasma sintered sample.

Temperature (°C)	Electrical resistivity (mΩcm)	Seebeck coefficient (μV/K)	Powerfactor (10^{-4} W/mK^2)
34.67765	1.305486	36.1535	1.001218
50.92236	1.325361	37.73655	1.07446
104.5498	1.404076	40.80417	1.185819
158.6704	1.466726	43.26117	1.27599
207.3055	1.521142	46.35359	1.412527
255.8773	1.574673	48.74901	1.50918
304.4798	1.623755	51.05098	1.605047
352.3582	1.655126	52.86539	1.688542
400.1436	1.708137	53.65612	1.68545
452.6097	1.774169	56.5494	1.80244

Table 16. Thermal conductivity for $Sr_8Ga_{16}Ge_{30}$, $Sr_8Ga_{16}Ge_{30}$ 2%Ba and $Sr_8Ga_{16}Ge_{30}$ 4%Ba, spark plasma sintered samples.

Temperature (°C)	Th. Cond. (W/mK) $Sr_8Ga_{16}Ge_{30}$	Th. Cond. (W/mK) $Sr_8Ga_{16}Ge_{30}$ 2%Ba	Th. Cond. (W/mK) $Sr_8Ga_{16}Ge_{30}$ 4%Ba
50	7.037607	8.080653	5.785955
100	6.959657	8.068871	5.924097
150	6.903955	8.045563	5.767665
200	6.808241	8.047865	5.60521
250	7.116484	7.936532	5.453704
300	7.017873	7.718049	5.22526
350	6.976872	7.472929	4.970486
450	7.213066	8.280641	5.587559

Table 17. Figure of merit for $Sr_8Ga_{16}Ge_{30}$, $Sr_8Ga_{16}Ge_{30}$ 2%Ba and $Sr_8Ga_{16}Ge_{30}$ 4%Ba, spark plasma sintered samples.

Temperature (°C)	Figure of merit $Sr_8Ga_{16}Ge_{30}$	Figure of merit $Sr_8Ga_{16}Ge_{30}$ 2%Ba	Figure of merit $Sr_8Ga_{16}Ge_{30}$ 4%Ba
50	0.000643	0.000596	0.000929
100	0.001347	0.001454	0.002002
150	0.002225	0.00242	0.003318
200	0.003332	0.003544	0.00504
250	0.004411	0.004459	0.006918
300	0.005612	0.006151	0.009215
350	0.007277	0.007405	0.01189
450	0.006095	0.007931	0.014516